

## ABSTRACT

Title of Thesis:                   MILLIGRAM-SCALE FLAME CALORIMETRY:  
NOVEL DESIGN OF A PYROLYZER SYSTEM  
USED TO EMULATE THE BURNING BEHAVIOR  
EXHIBITED BY COUPON-SIZED CONE  
CALORIMETRY SAMPLES

Jacques A. De Beer, Master of Science, 2020

Thesis Directed By:           Associate Professor Stanislav I. Stoliarov, Fire  
Protection Engineering

Milligram-scale Flame Calorimetry (MFC) is a controlled-atmosphere flammability technique used to screen fire retardant materials which do not intumesce. The MFC is a desirable technique due to its calorimetry capabilities, small sample size requirement and allowance for the non-intrusive study of an axisymmetric laminar diffusion flame. In in this work, a new MFC pyrolyzer system was developed to emulate the burning behavior of cone calorimetry samples, improving upon the limited use of the MFC. The new pyrolyzer system enables the testing of 30 – 55 mg samples as well as intumescent charring materials. The material surface temperature is directly measured during a test, which was previously not possible. A comparative study of five representative materials, covering a wide range of sooting and charring conditions, is conducted considering the new MFC, along with Microscale Combustion Calorimetry and cone calorimetry. It is concluded that the new MFC can be used to rank flammability of a wide range of polymeric materials and this ranking is the same at that obtained through cone calorimetry testing.

MILLIGRAM-SCALE FLAME CALORIMETRY: NOVEL DESIGN  
OF A PYROLYZER SYSTEM USED TO EMULATE THE  
BURNING BEHAVIOR EXHIBITED BY COUPON-SIZED CONE  
CALORIMETRY SAMPLES

by

Jacques A. De Beer

Thesis submitted to the Faculty of the Graduate School of the  
University of Maryland, College Park, in partial fulfillment  
of the requirements for the degree of  
Master of Science  
2020

Advisory Committee:

Professor Stanislav Stoliarov, Chair  
Dr. Fernando Raffan-Montoya  
Professor Peter Sunderland

© Copyright by  
Jacques A. De Beer  
2020

## Dedication

This work is dedicated to the late Kim James Yates. Your love and dedication for the field of fire forensics has inspired me to push my limits as a researcher. I am forever grateful for your support from the very beginning. Your legacy will never be forgotten.

## Acknowledgements

First, I would like to thank my family for their unwavering support. Moving to a foreign country to pursue a dream is never easy, but the love and support of my family has driven me to always put my best foot forward. Their continuous encouragement has made this entire experience easier and I can never thank them enough for everything they've done for me. Thank you.

Next, I would like to thank my advisor, Dr. Stanislav Stoliarov, for his guidance, encouragement and patience over the past two years. Dr. Stas, I am extremely appreciative of you giving me the opportunity to work with you. You have shown me what it really means to be a researcher, to work hard and strive for excellence. Thank you for your patience during the completion of this thesis. I am really looking forward to working with you for the next few years. Your support has given me the opportunity to pursue my dream.

I would also like to thank Dr. Fernando Raffan-Montoya for his support during this project. We started out as colleagues, but I am honored to be able to call you my friend. You have been there every time something went wrong with the MFC, discussing hypotheses and providing ideas. I hope this thesis does your previous work on the MFC justice.

I would like to thank Alyssa Kraus and the rest of her family for their support this past year. Alyssa, you have been there cheering me on since we first met. Your endless

love has inspired me to push my limits as an academic, as a person and as a loving partner. You mean the world to me.

I would like to thank my FPE research group for all their support during this project. Greg, Conor, Dushyant, Isaac, Josh, Yan, Lucas, Will, Hongen, Ryan, Ahmed and Evan, you have all played an integral role in my development as a researcher and as a person. I am extremely grateful for all your friendships.

Lastly, I would like to thank Dr. Peter Sunderland for accepting to serve on my committee. Thank you for giving your time to evaluate my current work. I look forward to potential collaborations in the future.

## List of Abbreviations

FPA: Fire Propagation Apparatus

HIPS: High-Density Polystyrene

HOC: Heat of Combustion

HRR: Heat Release Rate

LOI: Lower Oxygen Index

MCC: Microscale Combustion Calorimetry

MFC: Milligram-scale Flame Calorimetry

PMMA: Poly (methyl methacrylate)

PEEK: Poly (ether ether ketone)

PC: Polycarbonate

PVC: Poly (vinyl) chloride

SCCM: Standard Cubic Centimeter

SLPM: Standard Liter per Minute

UL: Underwriter Laboratories

# Table of Contents

Dedication .....	ii
Acknowledgements.....	iii
List of Abbreviations .....	v
Table of Contents.....	vi
List of Tables .....	viii
List of Figures.....	ix
1 Chapter 1: Introduction .....	1
1.1 Motivation.....	1
1.2 Flammability Testing Techniques.....	2
1.2.1 UL-94 Vertical Burning Test .....	2
1.2.2 Limited Oxygen Index .....	3
1.2.3 Microscale Combustion Calorimetry .....	5
1.2.4 Milligram-scale Flame Calorimetry.....	7
1.2.5 Cone Calorimetry.....	11
1.2.6 Fire Propagation Apparatus .....	14
1.2.7 Comparative Study of All Flammability Tests .....	16
1.2.8 Objective.....	19
2 Chapter 2: Development of a New Pyrolyzer System .....	21
2.1 New Pyrolyzer System Design .....	21
2.2 Power Supply .....	26
2.3 Nitrogen flowrate optimization.....	28
2.4 MFC Instrumentation Layout .....	31
2.5 Analysis of Power and Temperature Relationship.....	34
2.6 Heating Ramps.....	36
2.7 Pyrolyzer Coil Reproducibility .....	38
2.8 Temperature Calibration .....	39
2.9 MFC Processing Script .....	40
2.10 Summary of Pyrolyzer development .....	41
3 Chapter 3: Experimental Methodology.....	43



3.1	Material Specification, Preparation, and Test Matrix .....	43
3.1.1	Cone Calorimetry Sample preparation.....	46
3.1.2	Microscale Combustion Calorimetry Sample Preparation .....	47
3.1.3	Milligram-scale Flame Calorimetry Sample Preparation .....	48
3.2	Cone Calorimetry Experimental Methodology.....	51
3.3	MCC Experimental Methodology.....	53
3.4	MFC Experimental Methodology .....	56
4	Chapter 4: Results and Analysis .....	59
4.1	Cone Calorimetry Results .....	59
4.2	Microscale Combustion Calorimetry Results .....	69
4.3	Milligram-scale Flame Calorimetry Results.....	73
5	Chapter 5: Comparative analysis of Cone calorimetry, MCC and MFC data ....	82
5.1	Char yields .....	83
5.2	Normalized heats of combustion .....	84
5.3	Peak and average HRR .....	87
5.4	Ignition temperature and time-to-ignition.....	91
5.5	Smoke yield .....	96
6	Conclusions.....	99
7	Future Work .....	101
8	Bibliography .....	102

## List of Tables

Table 1.1: Comparative study of flammability measurement tests.....	17
Table 3.1: Materials studied in this work.....	43
Table 3.2: Chemical structure of studied materials. ....	44
Table 3.3: Test matrix for cone calorimetry, MCC, and MFC experiments.....	45
Table 3.4: Average sample mass and thickness used for the cone calorimeter experiments.....	47
Table 3.5: Average sample mass for the MCC experiments .....	48
Table 3.6: Average mass for granulated powder and disk-like plate samples prepared for MFC experiments.....	50
Table 3.7: Optical density as a function of the fraction of light transmitted .....	52
Table 4.1: Cone calorimeter results of duplicate tests for all sample materials tested at 50 kW m <sup>-2</sup> .....	68
Table 4.2: MCC combined experimental results considering a heating rate of 1 °C·s <sup>-1</sup> .....	73
Table 4.3: MFC experimental results for both sample geometries considering a maximum heat flux of 50 kW·m <sup>-2</sup> .....	81
Table 5.1: Comparison of ignition temperatures obtained from the MFC with that presented in the literature.....	94

## List of Figures

Figure 1.1: Experimental setup for the UL-94 Vertical Burning Test.....	3
Figure 1.2: Experimental setup for Limited Oxygen Index measurements .....	4
Figure 1.3: Experimental setup for cone calorimetry experiments.....	13
Figure 1.4: Experimental setup for fire propagation apparatus experiments.....	15
Figure 2.1: Pyrolyzer coil that was designed in-house with the use of 0.4 mm square nickel-chromium wire (a) and the ceramic holder housing the pyrolyzer coil (b), (c)22	
Figure 2.2: Zoomed-in view of the new MFC pyrolyzer coil system.....	23
Figure 2.3: Schematic diagram of the flat pyrolyzer coil/thermocouple system which will replace the Pyroprobe pyrolyzer .....	25
Figure 2.4: Idealized surface temperature profiles for cone calorimetry, MFC and MCC experiments.....	27
Figure 2.5: Pyrolyzate gases and airborne particulate condensation mass as a function of the purge gas flowrate with the pyrolyzer coil set at 30.8 W .....	29
Figure 2.6: MFC test with the axisymmetric diffusion flame present at the required position i.e. the lip of the crucible housing the pyrolyzer coil.....	31
Figure 2.7: Schematic diagram of the new MFC instrumentation layout.....	32
Figure 2.8: Temperatures profiles each with its corresponding coil power which was used during the operation of the MFC .....	35
Figure 2.9: Heating rate profiles for each with its corresponding coil power .....	36
Figure 2.10: Coil heating program highlighting both the Conditioning and Heating ramp used during an MFC experiment .....	37

Figure 2.11: Relation between the measured end temperature and the user-defined input voltage to the power supply using a co-flow of 100 SCCM N <sub>2</sub> .....	39
Figure 2.12: Calibration curve used to compensate for the thermal lag present between the thermocouple bead and the bottom surface of the sample within the ceramic crucible .....	39
Figure 2.13: Baseline measurement times considering temperature profile of a representative MFC experiment.....	41
Figure 3.1: Disk-like plates produced with the use of a 7 mm diameter hole punch. The samples from left to right are: PMMA, HIPS, PC, PEEK, and PVC .....	49
Figure 3.2: Schematic layout of the MCC instrumentation .....	54
Figure 4.1: Cone calorimetry HRR profiles at an incident heat flux of 50kW/m <sup>2</sup> , using samples with thicknesses ranging from 2.8 – 3.05 mm .....	61
Figure 4.2: Cone calorimetry MLR profiles at an incident heat flux of 50 kW/m <sup>2</sup> , using samples with thicknesses ranging from 2.8 – 3.05 mm .....	62
Figure 4.3: Cone calorimetry smoke production profiles at an incident heat flux of 50 kW/m <sup>2</sup> , using samples with thicknesses ranging from 2.8 – 3.05 mm .....	65
Figure 4.4: Photographs of final solid residue obtained in cone calorimeter experiments .....	65
Figure 4.5: Cone calorimetry instantaneous HOC profiles at an incident heat flux of 50 kW/m <sup>2</sup> used to calculate the HOC as normalized by the gasified mass .....	67
Figure 4.6: Criteria used to determine the onset HRR temperature for all the MCC tests which also indicates the limits of integration for each material .....	70

Figure 4.7: MCC HRR profiles for granulated powders and sample shavings for a heating rate of 1 °C/s up to 750 °C as normalized by the initial sample mass .....	71
Figure 4.8: MFC HRR profiles as normalized by the initial sample mass for granulated powder- and disk-like plate samples for each material obtained using Method B after the initiation of the Heating ramp .....	76
Figure 4.9: Measured surface temperature profiles and the corresponding heating rate profiles for both sample geometries of each material in the MFC .....	79
Figure 5.1: Char yields for the (a) MFC and (b) MCC compared to the yields obtained in the cone calorimeter.....	84
Figure 5.2: HOC data for (a) MFC and (b) MCC experiments as normalized by the initial sample mass and compared to the values obtained in the cone calorimeter.....	86
Figure 5.3: HOC data for (a) MFC and (b) MCC experiments as normalized by gasified mass of the sample and compared to the values obtained in the cone calorimeter.....	87
Figure 5.4: Peak HRR values from the cone calorimeter compared with peak HRR values for (a) MFC, (b) MCC .....	89
Figure 5.5: Peak HRR as a function of the time to ignition for both MFC sample geometries.....	90
Figure 5.6: Relation between ignition times obtained from cone calorimeter experiments and the ignition temperatures obtained from (a) MFC experiments, (b) the onset HRR temperatures from MCC experiments .....	93
Figure 5.7: Onset HRR temperatures from the MCC experiments compared to the ignition temperatures from the MFC experiments.....	96

Figure 5.8: MFC particulate yield compared to the average extinction area calculated from cone calorimeter experiments ..... 97

# 1 Chapter 1: Introduction

## 1.1 *Motivation*

The use of polymeric materials in the built environment has become increasingly more popular, replacing traditional materials as a viable alternative [1]. The availability of raw materials for manufacturing, ease of processing and controllable physical properties of these polymeric materials are some of the key features attributed to their widespread use [2]. One of the most notable drawbacks related to the use of these materials is that the majority of polymers are organic and therefore inherently flammable [3]. The ever-increasing use of polymeric materials requires that the flammability properties of these materials are understood and accurately quantified, enabling end users to make well-informed decisions when selecting adequate materials for a particular application.

There are bench- and milligram-scale flammability tests that can be used to calculate different flammability parameters for polymers. The parameters that have been identified to form the basis in estimating the hazard of a material when exposed to fire are ignitability, flame spread, heat release and smoke yield. Flammability tests that are of particular importance when considering flammability testing of polymeric materials include the UL 94 Vertical Burning Test, the Limited Oxygen Index Test, Cone Calorimetry, the Fire Propagation Apparatus, Microscale Combustion Calorimetry, and Milligram Scale Flame Calorimetry [4]. Knowledge about each of

these test methods is required to ensure that the correct test method is selected to adequately quantify or rate the flammability of a material, all while considering the limitations of these tests.

## 1.2 Flammability Testing Techniques

### 1.2.1 *UL-94 Vertical Burning Test*

The UL-94 flammability test is a test that is used to assess the flame resistance of synthetic polymer materials with the test being standardized as ASTM D3801 [5]. The test method comprises a bench-scale procedure that is used to determine the tendency of a material to spread flame or extinguish when exposed to a premixed pilot flame with a length of 20 mm (50 W) that is applied to the base of the sample as per Figure 1.1 [5]. Each material that is tested is tested as a set of 5 samples (13 mm x 125 mm) with the thickness of the sample no greater than 13 mm. Once the flame of the hand-held Bunsen burner is applied to sample, the extent and duration of burning is used to rate a material. The material ratings for the vertical configuration of the UL-94 test is V-0, V-1, V-2 (listed from least to most flammable) and 'Fail' as outlined in ASTM D3801.



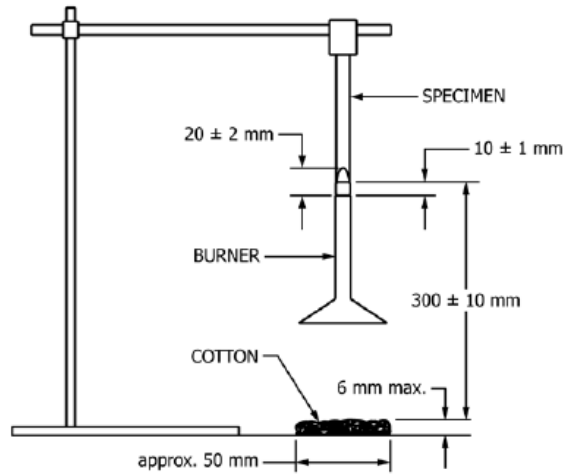


Figure 1.1: Experimental setup for the UL-94 Vertical Burning Test [5]

The advantages of using this test is that it provides a qualitative measure to rate the flammability of materials with only relatively small samples (25 – 30 g) required to run the test. The disadvantages of this test, however, are as follows: it is visually evaluated, it only measures the dripping and burning rate of a material, the rating is dependent on the thickness of the sample, UL-94 is not a well-ventilated test, and UL-94 measures the burning behavior of a material when exposed to an external heat source for a 10 second period [6]. The UL-94 test also has the disadvantage of being laborious and time-consuming.

### 1.2.2 Limited Oxygen Index

The Limited Oxygen Index (LOI) fire-test-response standard is related to the minimum oxygen concentration required to sustain flaming combustion of a material in an oxygen/nitrogen atmosphere. The test was first introduced by Fenimore and Martin in 1966 and has been standardized as ASTM D2863 in the United States and

ISO 4589 internationally [7]. The test comprises a vertically-mounted sample (10 – 20 g) that is ignited at its top edge as per Figure 1.2. The oxygen flowrate is adjusted until a critical concentration is obtained under which flaming combustion is not supported [8].

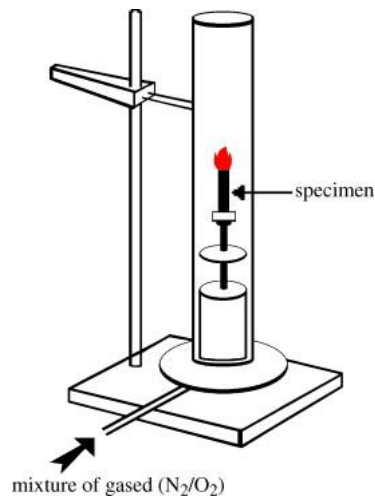


Figure 1.2: Experimental setup for Limited Oxygen Index measurements [9]

The value of the LOI is defined as the minimum oxygen concentration where flaming combustion is maintained, in a mixture of oxygen and nitrogen, for a minimum of 3 minutes or the minimum concentration of oxygen where 5 cm of the sample is consumed. The material is classified as “combustible” if the LOI is calculated to be less than 21% and “self-sustaining” if the LOI is greater than 21%, indicative of combustion that cannot be sustained at ambient conditions without the use of an external heat source.[9].

The advantages of using the LOI test is that it provides end-users with the means to determine a reproducible quantitative measure of a materials’ flammability. The

equipment used in the test is also inexpensive and only relatively small sample sizes (10 – 20 g) are required. However, the test has a few drawbacks in that dripping and melting during a test can cause extinguishment of a sample resulting in high LOI values. It has also been noted that as a result of the test being conducted at room temperature, calculated LOI values will be smaller than that at elevated temperatures. This means that materials with high LOI values at room temperature could, in fact, burn without self-extinguishing when exposed to real-life fire conditions. The oxygen percentage in the mixture is varied to maintain a candle-like flame which does not emulate the burning conditions of a material during a real fire [7].

### *1.2.3 Microscale Combustion Calorimetry*

Fire behavior and flame resistance of polymeric materials at the macroscopic scale depend on sample size, orientation, contributing thermophysical and thermochemical properties and environmental parameters [10] which results in these parameters being classified as extrinsic properties of the material. The Federal Aviation Administration (FAA) has developed a test method, Microscale Combustion Calorimetry (MCC), that can be used to measure the intrinsic properties of a material. MCC is a standard test method used to calculate the complete heat of combustion of a material and it is available as ASTM D7309 [11].

The MCC test is used to measure the complete heat of combustion of the volatile gases produced during the thermal decomposition of the material as calculated considering the oxygen consumption technique. The oxygen consumption calorimetry

technique is based on the empirical observations made by Huggett [22]. Huggett noted that for most polymeric materials,  $13.1 \pm 0.6 \text{ kJ}\cdot\text{kg}^{-1}$  of energy is released per kilogram of oxygen consumed. The volatiles are produced during the controlled heating of a milligram-sized sample [10]. The process of condensed-phase fuel generation and gas-phase flaming combustion is separately reproduced. The thermal decomposition process is driven to completion, allowing the measurement of the complete heat of combustion of the material [12]. The MCC test procedure comprises the use of samples with a mass ranging from 1 – 10 mg which is weighed into a ceramic crucible. It is then inserted and sealed into the pyrolyzer, with a standard set point temperature of 750 °C and heated up to this point at a rate of 1 °C/s with the combustor temperature set to 900 °C. The standard calls for the use of either Method A or Method B, with Method A entailing an anaerobic thermal decomposition process and Method B that of a thermo-oxidative decomposition process. In Method A, the condensed-phase fuel generation process is emulated in the pyrolyzer section of the MCC with the production of volatile decomposition products in a nitrogen environment. These decomposition products are then swept into the combustor, using a purge gas, where the volatile products are completely oxidized emulating the gas-phase flaming combustion process. The combustion gas stream is scrubbed upstream of a mass flow meter and oxygen analyzer where water and acid gases are removed.

MCC is an attractive flammability test as it requires small sample sizes, which is advantageous when used for material screening purposes. It is also a valuable tool that can be used for modelling purposes [13–15] There are, however, limitations when

using the MCC which are summarized as follows: there is no real flaming combustion inside the combustor which may yield different results than an actual flaming combustion process, and the use of a small sample size does not accurately represent the physical effects (dripping or intumescence) of large burning samples. The sample size variations can also have an effect on the measured peak heat release rate (PHRR) due to the controlled amount of oxygen present in the combustor [16].

#### *1.2.4 Milligram-scale Flame Calorimetry*

Milligram-scale Flame Calorimetry (MFC) is a test method that was developed at the University of Maryland, College Park and is used as a quantitative tool to screen flame retardants and synergists. The test method makes use of milligram-sized samples, on the order of 30 – 40 mg, and yields valuable data regarding the flammability of a material [17]. The use of the MFC for screening purposes during material development is desirable due to it requiring a small sample mass, its calorimetry capabilities, as well as allowing for the non-intrusive study of an axisymmetric laminar diffusion flame.

The MFC allows for the calculation of the heat of combustion of a material during the anaerobic decomposition of the sample. This is done considering the heat release rate (HRR) normalized by the initial sample mass of a material during a test and integrating this parameter over time. The solid products of combustion (airborne particulates) yield and solid residue (char) yield of the thermally decomposing sample can also be determined. The MFC is successfully used to detect the gas-phase effect

that flame retardants have on the flaming combustion process of a material [17] as well as measure the radiative fraction for solid fuels [18].

The MFC test procedure comprises the use of a sample which is weighed into a transparent quartz sample crucible with an inner diameter of 4 mm and a length of 14 mm. A gas mixture (usually air) is fed into the system providing the atmosphere for the samples to burn in. A purge gas, usually nitrogen, is introduced into the system via the quartz tube enclosing the pyrolyzer coil and is used as a carrier gas to assist the movement of pyrolyzates to the igniter, located above the lip of the quartz tube. Here, the hot-wire igniter initiates flaming combustion once there is an adequate fuel/air ratio to sustain a diffusion flame. The sample is heated at a user-defined linear heating rate, usually  $10\text{ }^{\circ}\text{C}\cdot\text{s}^{-1}$  up to a temperature of  $1200\text{ }^{\circ}\text{C}$  using a commercially available Pyroprobe pyrolyzer. A filter is used to retain all the airborne particulates produced during the flaming combustion of the sample. Downstream of the particulate filter, the exit flowrate and oxygen concentrations are measured simultaneously, followed by the measurement of the CO and CO<sub>2</sub> concentrations.

The MFC relies on the oxygen consumption technique which considers Huggett's empirical observations [22] to calculate the heat release rate of a burning fuel. When calculating the heat release rate of a material, only the instantaneous oxygen consumption rate is required and assuming the absence of any product storage processes within the MFC, the rate of oxygen consumption can be expressed per Equation 1. Both terms on the right hand side of Equation (1 represent the oxygen mass flowrates at the inlet,  $(\dot{m}_{O_2})_{IN}$ , and outlet,  $(\dot{m}_{O_2})_{OUT}$ , of the combustor respectively.

The flowmeter downstream of the particulate filter in conjunction with the oxygen sensor can be used to calculate the oxygen mass flowrate from the combustor as per Equation (2).

$$\Delta\dot{m}_{O_2} = (\dot{m}_{O_2})_{IN} - (\dot{m}_{O_2})_{OUT} \quad (1)$$

$$(\dot{m}_{O_2})_{OUT} = \rho_{O_2} \dot{V}_{OUT} [O_2]_{OUT} \quad (2)$$

The density of the oxygen gas as represented by  $\rho_{O_2}$  ( $\text{kg}\cdot\text{m}^{-3}$ ) was taken at standard temperature and pressure conditions (25 °C and 1 atm);  $[O_2]_{out}$  is the volumetric fraction of oxygen at the outlet of the combustor,  $\dot{V}_{OUT}$  is the instantaneous volumetric flowrate in  $\text{m}^3\cdot\text{kg}^{-1}$ ,  $(\dot{m}_{O_2})_{IN}$  and  $(\dot{m}_{O_2})_{OUT}$  are the mass flowrate of oxygen at the inlet and outlet of the system, respectively, in  $\text{kg}\cdot\text{s}^{-1}$ , and  $\Delta\dot{m}_{O_2}$  is the difference in the mass flowrate between the inlet and outlet streams in  $\text{kg}\cdot\text{s}^{-1}$  [19].

The first method that is used to calculate the heat release rate is referred to as Method A with this method more accurately representing the global processes within the MFC. For this method, the following assumptions pertaining to the inlet flowrate are made: if compressed air is used as the co-flow gas, the mass flowmeter and oxygen sensor, downstream of the combustor, can be used to measure the inlet oxygen flowrate during steady, non-combustion operation of the MFC. It is further assumed that the inlet flowrate of oxygen remains constant as the flowrate of this stream is controlled with the use of a separate mass flow controller. Method B, the second method, makes use of the assumption that the inlet oxygen volume fraction remains constant for the

duration of the test, but the total inlet flowrate instantaneously matches that measured at the outlet. This assumption is also used in the MCC method [10] to calculate the HRR of a pyrolyzing sample and Equation (1 then becomes:

$$\Delta\dot{m}_{O_2} = \rho_{O_2}\dot{V}_{OUT}([O_2]_{IN} - [O_2]_{OUT}) \quad (3)$$

In a further study, Raffan-Montoya et al. [19] revised the calculation of the two methods used to calculate the change in oxygen mass flowrate through the system. This revision included a correction for the measured volumetric flowrate such to compensate for the flow at the outlet having a different composition than air. This difference in composition had to be accounted for to ensure that the correct flowrate readings were obtained. The reader is referred to an earlier publication [19] providing further detail about the procedure used to calculate the true outlet volumetric flowrate. In summary, the true volumetric flowrate is calculated considering the Hagen-Poiseuille equation whilst considering the dynamic viscosity of the outlet flow as per Equation (4.

$$\dot{V}_{true} = \dot{V}_{meas} \frac{\mu_{air}}{\mu_{true}} \quad (4)$$

With  $\mu_{air}$  and  $\mu_{true}$  being the dynamic viscosity of air (Pa·s) and the true dynamic viscosity of the outlet flow in  $\text{kg}\cdot\text{m}^{-1}\cdot\text{s}^{-1}$ . The outlet flow was assumed to comprise a mixture of  $O_2$ ,  $CO_2$  and  $N_2$  and the dynamic viscosity of the mixture was calculated considering Equation (5.

$$\mu_{mix} = 0.5 \left( \sum_i \mu_i x_i + \frac{1}{\sum_i \frac{x_i}{\mu_i}} \right) \quad (5)$$



where  $\mu_i$  and  $x_i$  is the dynamic viscosity and molar fraction of each component. The viscosity for the gases was retrieved from National Institute for Standards and Technology (NIST) databases [20].

The limitations and disadvantages of the MFC are as follows: The quartz test tube that is used is 14 mm tall, with an outer diameter of 6 mm. This test tube provided a physical problem in that the test tube tended to clog when highly charring or intumescent materials were being tested. This resulted in a compromised HRR curve and subsequent calculated heat of combustion value for the material being considered. Another limitation of the test tube was that only granulated or small sample shavings could be tested. The temperature of the sample during the test was not measured and thus an additional test had to be conducted to obtain the surface temperature of the sample during the test with the use of a thermocouple inserted into the test tube, thereby providing an additional physical disadvantage of the MFC. The sample mounted in the test tube was heated using a commercially available pyroprobe pyrolyzer, CDS 5000, with the business end of the probe housing a platinum spiral coil. The cost of the CDS 5000 pyroprobe pyrolyzer is large and presents another significant disadvantage.

### *1.2.5 Cone Calorimetry*

Cone calorimetry is one of the most effective reaction-to-fire bench-scale tests used to quantify the fire behavior of a material when exposed to controlled levels of radiant heating with or without an external ignition source. Cone calorimetry makes use of the oxygen consumption calorimetry technique which entails the measurement of the

instantaneous change in oxygen concentration in the combustion gases of a sample when exposed to a given heat flux, typically 10 to 100 kW·m<sup>-2</sup> [21]. The cone calorimeter has been adopted by both the International Organization of Standardization (ISO DIS 5660) and ASTM (E 1354) as the bench-scale method used to measure the HRR of a material. The samples that are used for cone calorimetry tests comprise 100 by 100 mm squares, having a thickness no greater than 50 mm. The flammability parameters that are calculated from cone calorimetry experiments are time to ignition, the HRR of the burning material as a function of the duration of the test, the heat of combustion of a material normalized by both the initial sample mass and the gasified mass, and the char yield [23].

The study of smoke developed by fire is important in fire protection and is defined as a mixture of solid particulates, volatile organic compounds and liquid and gaseous inorganic compounds [24]. Smoke particulates that are generated during the burning of a material acts as a radiating medium that can potentially affect the heat flux distribution of a fire [25]. The most popular optical property is the smoke extinction coefficient which can be used to determine the mass concentration of flame-generated smoke which is obtained using light extinction measurements [26].

The calculation of the light extinction coefficient is based off Bouger's law that relates the intensity of the incident monochromatic light of a specific wavelength to the intensity of the light transmitted through a defined path length of smoke [23]. Bouger's law is expressed as per Equation (6):

$$I/I_0 = e^{(-kL)} \quad (6)$$

where  $I$  and  $I_0$  are the intensity of the blocked and monochromatic light respectively.  $L$  is the selected path length (m) and  $k$  the extinction coefficient,  $m^{-1}$ . The instrumentation layout of the cone calorimeter is depicted per Figure 1.3.

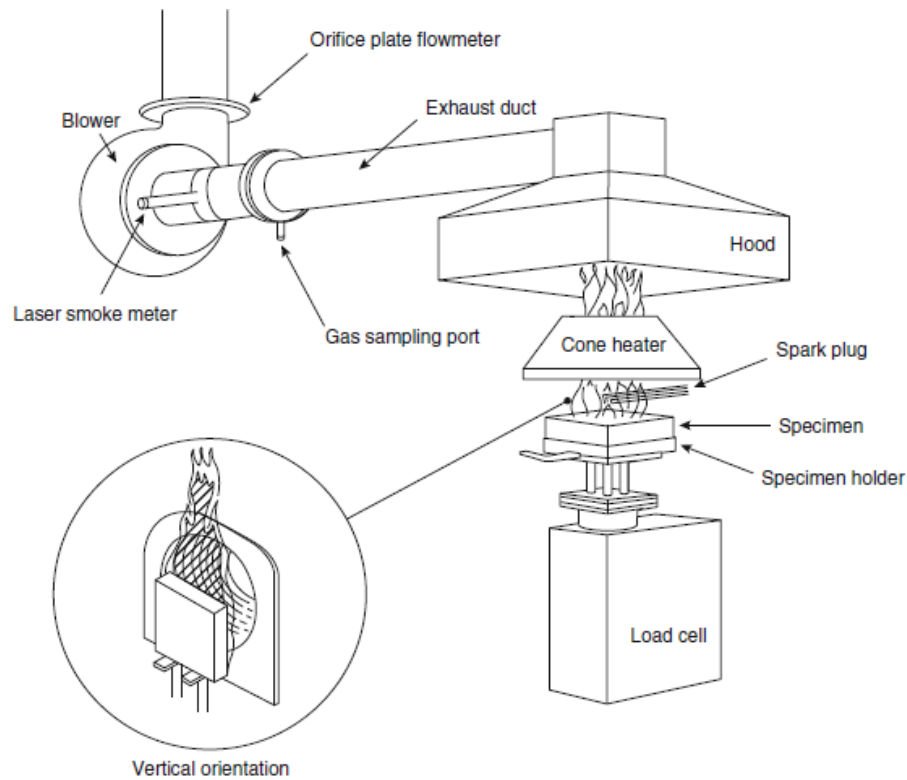


Figure 1.3: Experimental setup for cone calorimetry experiments [24]

Considering all the material properties and flammability parameters that can be determined using cone calorimetry, there are still limitations to this test that should be considered: the size of the samples used for cone calorimetry tests are large (30 – 50 g) in comparison to size of samples used in the MCC (3 – 10 mg) or MFC (30 – 50 mg).

The large sample size used for cone calorimetry tests is not favorable when screening materials during new product development. Swelling of the sample prior to ignition will potentially interfere with the spark igniter. Significant swelling of the sample during the test can result in different incident heat flux profiles along the height of the swelling sample. Spalling can compromise the validity of the test and adequate ventilation must be ensured.

### *1.2.6 Fire Propagation Apparatus*

The Fire Propagation Apparatus (FPA) is used to evaluate the flammability of materials; however, unlike the cone calorimeter, the heat is supplied by infrared tungsten heating lamps. The FPA also provides control over the oxygen environment around the sample, allowing for the testing of both under- and well-ventilated fire conditions. The FPA has been standardized in accordance with ISO 12136 and ASTM E2058. Samples are exposed to incident radiant heat fluxes up to  $65 \text{ kW m}^{-2}$  with ignition obtained using a pilot flame of an ethylene-air composition. Samples, when tested in the horizontal configuration are square shaped with a 101.6 by 101.6 mm area and a thickness not exceeding 25.4 mm. Vertical tests comprise the use of planar samples with a width of 101.6 mm and a length of 305 mm. The thickness of the samples ranges from 3 to 13 mm [27].

The standard, ASTM E2058, calls for the use of three separate tests to obtain different flammability characteristics of a material and are as follows: the time-to-ignition of a material, the chemical and convective HRR, the mass loss rate (MLR), the

heat of combustion (HOC), and the smoke production. This test is different from other flammability tests in that the chemical HRR during and after self-sustaining, upward flame propagation on a vertically-mounted sample can be determined using an inlet air stream with a 40% oxygen concentration, in the absence of an external radiant heat flux. The instrumentation layout of the FPA is depicted per Figure 1.4.

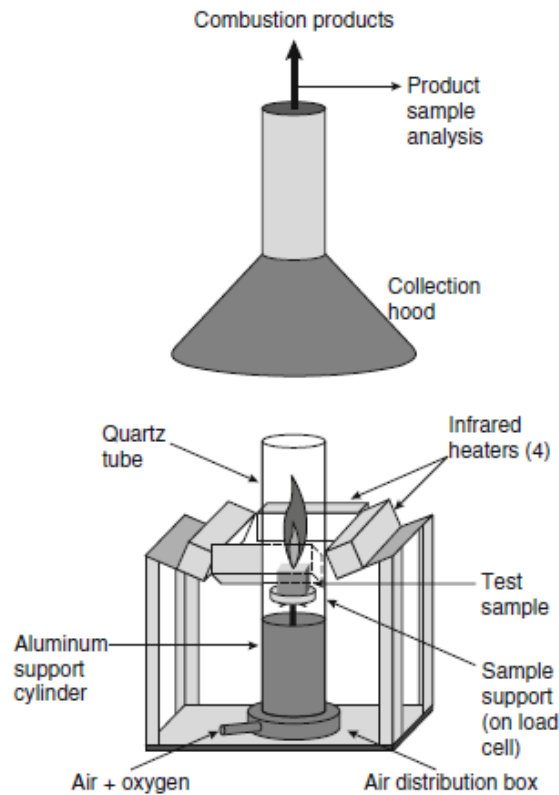


Figure 1.4: Experimental setup for fire propagation apparatus experiments

The main advantage of the FPA is that the air composition around the sample can be controlled, allowing for the testing of samples in both under- and well-ventilated conditions. The control of the air compositions allows for the testing of a vertically mounted sample at an oxygen concentration of 40% which is required to emulate the

radiant heat flux from real-fire flames [24]. However, the large sample sizes required by the standard is a disadvantage when screening materials during material development. Another limitation is the requirement of the standard to conduct three separate tests methods to obtain flammability parameters, most of which can be obtained with a single test using cone calorimetry. The multitude of test methods also makes this standardized test laborious and time-consuming.

### *1.2.7 Comparative Study of All Flammability Tests*

A comparative study of all the above-mentioned flammability measurement tests was conducted to highlight the advantages and limitations as well as the difference in sample size for each of the tests as per Table 1.1. It should be noted that LOI was the first of considered flammability testing techniques used (1970) and was followed by the approval of UL-94, cone calorimetry, FPA, MCC and then MFC (2015). The deficiencies and advantages of the above-mentioned standard tests preceding the development of the MFC were considered to warrant the initial development of the MFC. This, in turn, would highlight how some of these deficiencies were addressed through the development of the MFC. The advantages and limitations of each test are presented in Table 1.1.

One of the main limitations of most of the tests, with the exclusion of MCC and MFC, is the size of the sample required by the standard. The sample size for all these tests, while relatively small compared to a real fire scenario is still relatively large for screening campaigns or when testing novel materials whose production is still at the

R&D scale. For this reason, the MCC was developed to allow for the testing of sample masses on the order of milligrams (1 – 10 mg). Although the MCC decouples the gas- and condensed phase processes of pyrolysis and flaming combustion, no real flaming combustion process is ever present within the combustor of the MCC. Both cone calorimetry, being the benchmark flammability standard, and FPA tests are conducted considering the real flaming combustion of samples with an advantage of an experiment in the FPA being conducted in a controlled atmosphere. The MFC was developed considering the limitations as highlighted for MCC, cone calorimetry and the FPA. The MFC was developed to allow for testing of milligram sized samples on the order of 30 – 50 mg, while accommodating flaming combustion of a material in a controlled atmosphere. The calorimetry capability of MFC makes it a test that allows for the direct calculation of the HRR, the non-intrusive study of the flame as well as the measurement of the solid residue yield and solid products of combustion yield.

Table 1.1: Comparative study of flammability measurement tests

Test	Sample size	Advantages	Limitations
UL-94V (1978)	125 x 12.5 mm Thickness < 13 mm	<ul style="list-style-type: none"> <li>• Qualitative rating of flammability</li> <li>• Small sample sizes</li> </ul>	<ul style="list-style-type: none"> <li>• Visual evaluation</li> <li>• Only burning rate and dripping measured</li> <li>• Rating dependent on sample thickness</li> <li>• External heat source only applied for 10 s</li> </ul>
LOI (1970)	150 x 10 mm Thickness: 10.5 mm	<ul style="list-style-type: none"> <li>• Measured critical oxygen concentration required to sustain flaming combustion</li> </ul>	<ul style="list-style-type: none"> <li>• Dripping and melting compromises test</li> <li>• LOI is surrounding temperature-dependent</li> </ul>

MCC (2007)	1 – 10 mg	<ul style="list-style-type: none"> <li>• Small sample sizes</li> <li>• Complete HOC measured</li> <li>• Small sample size</li> <li>• Sample surface temperature is directly measured</li> </ul>	<ul style="list-style-type: none"> <li>• Candle-like flame doesn't emulate real fire conditions</li> <li>• No real flaming combustion</li> <li>• Complete combustion process overrides physical processes</li> <li>• PHRR depends on sample size</li> </ul>
Cone (1990)	100 x 100 mm Thickness < 50 mm	<ul style="list-style-type: none"> <li>• Adopted as the test used to measure HRR</li> <li>• MLR is directly measured</li> <li>• Allows for smoke obscuration measurements</li> <li>• Large heat flux range available for testing</li> </ul>	<ul style="list-style-type: none"> <li>• Sample sizes are large</li> <li>• Intumescence of materials can interfere with igniter</li> <li>• Varying incident heat flux profiles when samples swell</li> <li>• Spalling can compromise test validity</li> <li>• Proper ventilation required</li> </ul>
FPA (2000)	101.6 x 106.1 mm Thickness < 25.4 mm	<ul style="list-style-type: none"> <li>• Air composition around sample can be controlled</li> <li>• Radiant heat flux from real fires can be emulated</li> <li>• Non-intrusive study of flame</li> </ul>	<ul style="list-style-type: none"> <li>• Sample sizes are large</li> <li>• Test comprises 3 methods required to obtain all flammability parameters</li> </ul>
MFC (2015)	30 – 40 mg	<ul style="list-style-type: none"> <li>• Effective HOC measured</li> <li>• Small sample size</li> <li>• Non-intrusive study of flame</li> <li>• High heating rate similar to real fire conditions</li> </ul>	<ul style="list-style-type: none"> <li>• Clogging of quartz test tube when testing charring materials</li> <li>• Only granulated powder/sample shavings can be used</li> <li>• Surface temperature is not measured during test</li> </ul>



- 
- |  |  |   |
|--|--|---|
|  | <ul style="list-style-type: none"><li>• Successful detection of gas-phase combustion effects</li></ul> | <ul style="list-style-type: none"><li>• Pyroprobe pyrolyzer is expensive and does not emulate heating conditions seen in cone calorimetry</li></ul> |
|--|--|---|
- 

### 1.2.8 Objective

Currently, cone calorimetry is viewed as the benchmark test used to quantitatively characterize the flammability of a material. Cone calorimetry, as with every flammability testing technique, has its own limitations, such as the requirement of relatively large sample sizes (30 – 50 g), the need for well-ventilated conditions, and the test being time-consuming or laborious. The MCC test was developed to alleviate the limitation of a large sample mass by using milligram samples sizes (3 – 10 mg) but being limited but not accurately emulating the flaming combustion behavior representative of real fire scenarios. The MFC was, in turn, developed, to address the need for a milligram-scale test that can be used to study the flaming combustion process of a material in a controlled environment. The MFC does however have inherent disadvantages in that the test is, for the most part, only used to screen materials during material development without accurately emulating the burning behavior of materials as seen during cone calorimetry experiments. The test was limited to non-charring materials due to the limited size of the sample crucible, and the surface temperature of the material cannot be measured during a controlled-environment test.

Considering these limitations and disadvantages, the objectives of this study were to design a new MFC pyrolyzer system such that the heating conditions more closely emulate the burning behavior of materials in the cone calorimeter while still controlling

the flaming combustion atmosphere within the MFC combustor chamber. The MFC experimental setup will be modified in such a way as to reduce the cost of the pyrolyzer, alleviate the tendency of charring materials clogging the sample crucible, measure the surface temperature of the sample during a test and more closely replicate the heating conditions and ignition theory observed during cone calorimetry experiments. A material matrix comprising five materials, representative of a large range of synthetic polymers, will be tested in the MFC with the new pyrolyzer system, as well as in MCC and the cone calorimeter. The results from these tests will be directly compared to determine how the results of these tests quantitatively correlate with one another.

## 2 Chapter 2: Development of a New Pyrolyzer System

### 2.1 New Pyrolyzer System Design

The pyrolyzer system that is used in the MFC is one of the most important components of the instrument, as this component has a direct impact on the heat release rate, char yield and particulate yield of the system. The pyrolyzer heating coil was designed with the use of 0.4 mm square nickel-chromium wire. The shape of the pyrolyzer coil was changed from the originally-used spiral configuration to a flat radial configuration as per Figure 2.1a. The flat radial pyrolyzer coil had an outer diameter of 9.6 mm with an interior circular opening of 4 mm. Both ends of the pyrolyzer coil were fitted with a female D-Sub socket contact crimps with a gauge ranging from 20 – 24 AWG. The contact material comprised a copper alloy with a gold contact finish. This coil was housed within a circular ceramic holder and was fixed in place using Autocrete High-temperature ceramic adhesive as depicted per Figure 2.1b, c. The 3.56 mm diameter interior hole of the ceramic holder housed the thermocouple insulator that was fixed in-place. The resistance of the pyrolyzer coil was measured as 0.6 ohm and had a length of 100 mm.

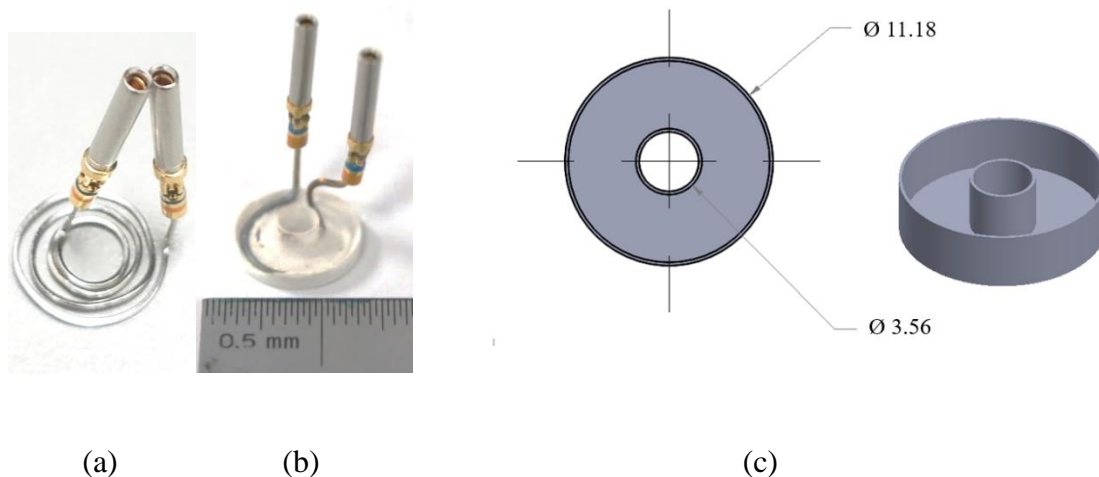


Figure 2.1: Pyrolyzer coil that was designed in-house with the use of 0.4 mm square nickel-chromium wire (a) and the ceramic holder housing the pyrolyzer coil (b), (c)

The new pyrolyzer system with all relevant dimensions is depicted per Figure 2.2. The ceramic crucible housing the sample is positioned on top of the ceramic holder housing the pyrolyzer coil leaving a 2.5 mm clearance between the lip of the crucible and the lip of the quartz tube housing the pyrolyzer coil system. This distance was deemed adequate to allow for the purge gas to aid in the transport of the pyrolyzate gases towards the ignitor while also reducing the possibility of the intumescent char touching the hot wire igniter. The hot wire igniter was positioned 2 mm above the lip of the quartz tube housing the pyrolyzer coil and just over the interior edge of said quartz tube. This aids in ignition of the gaseous pyrolyzates, while not being intrusive to such an extent as to compromise the geometry of the flame. An Omega 0.08 mm wire diameter K-type thermocouple with fiberglass cable insulation and an exposed junction was used. The thermocouple was installed flush against the top surface of the ceramic thermocouple insulator with both holes of the insulator being sealed using the

high-temperature ceramic adhesive. This was done to protect the thermocouple wiring from thermal insult induced by the flat radial pyrolyzer coil and to eliminate the possibility of gas leaks through the insulator holes during a closed-system test. A zoomed-in view of the final setup of the new pyrolyzer heating coil in relation to the thermocouple bead is depicted in Figure 2.2. The new pyrolyzer system comprises the in-house designed flat radial pyrolyzer coil, as well as the 0.08 mm bead diameter K-type thermocouple is schematically represented per Figure 2.3

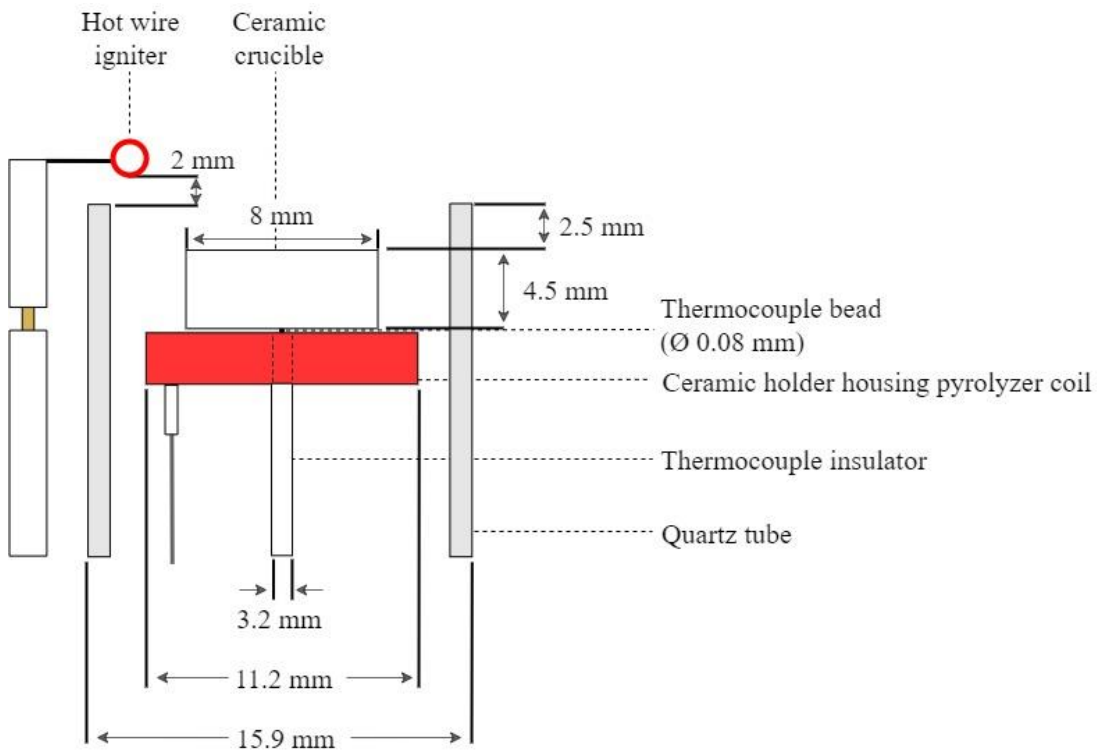


Figure 2.2: Zoomed-in view of the new MFC pyrolyzer coil system

It was crucial that the thermocouple bead was installed flush with the bottom exterior surface of the circular ceramic housing for two main reasons: to minimize the effect of thermal lag in the system and to ensure that there is proper thermal contact

between the thermocouple bead and the ceramic sample crucible. The ceramic adhesive that was used to fix the thermocouple in place required a curing period of at least 24 hours.

The pyrolyzer system that replaced the original pyroprobe pyrolyzer system is depicted in Figure 2.3. The flat radial pyrolyzer coil was housed in a 15.88 mm (5/8 in.) outer diameter quartz tube, having an inner diameter of 13 mm. The diameter of the quartz tube was selected to allow for a gap between the outer edges of the flat pyrolyzer coil and the quartz tube, thereby allowing the purge gas to readily flow upwards past the pyrolyzer coil. The quartz tube diameter was also favorable as it could readily fit into a 15.88 mm Swagelok threaded nut and be sealed using a nylon ferrule. The thermocouple was housed in a 0.305 m long ceramic thermocouple insulator (3.2 mm diameter) which extends through a Swagelok 15.88 mm male union tee. The thermocouple insulator was mounted in place and sealed at the bottom exposed end using a 3.18 mm diameter PTFE ferrule (see Figure 2.3, number 9). This way of mounting ensured that the pyrolyzer coil system did not move during a test and that the pyrolyzer coil was centered in the housing quartz tube, allowing evenly distributed flow across the radial length of the pyrolyzer coil.

The electrical cable used to power the pyrolyzer coil (see Figure 2.3, number 13) extended from the base of the pyrolyzer coil down through the first union tee. It exited the pyrolyzer system through the 15.88 mm diameter spherical ferrule (see Figure 2.3, number 14). The nitrogen purge gas was introduced into the system via a 15.88 mm diameter PVC tube, as per the previous design of the MFC [19]. The entire

pyrolyzer system was sealed to eliminate the escape of any gases through any connections in the pyrolyzer system, with the cylindrical ferrule being sealed with the use of a silicone sealant.

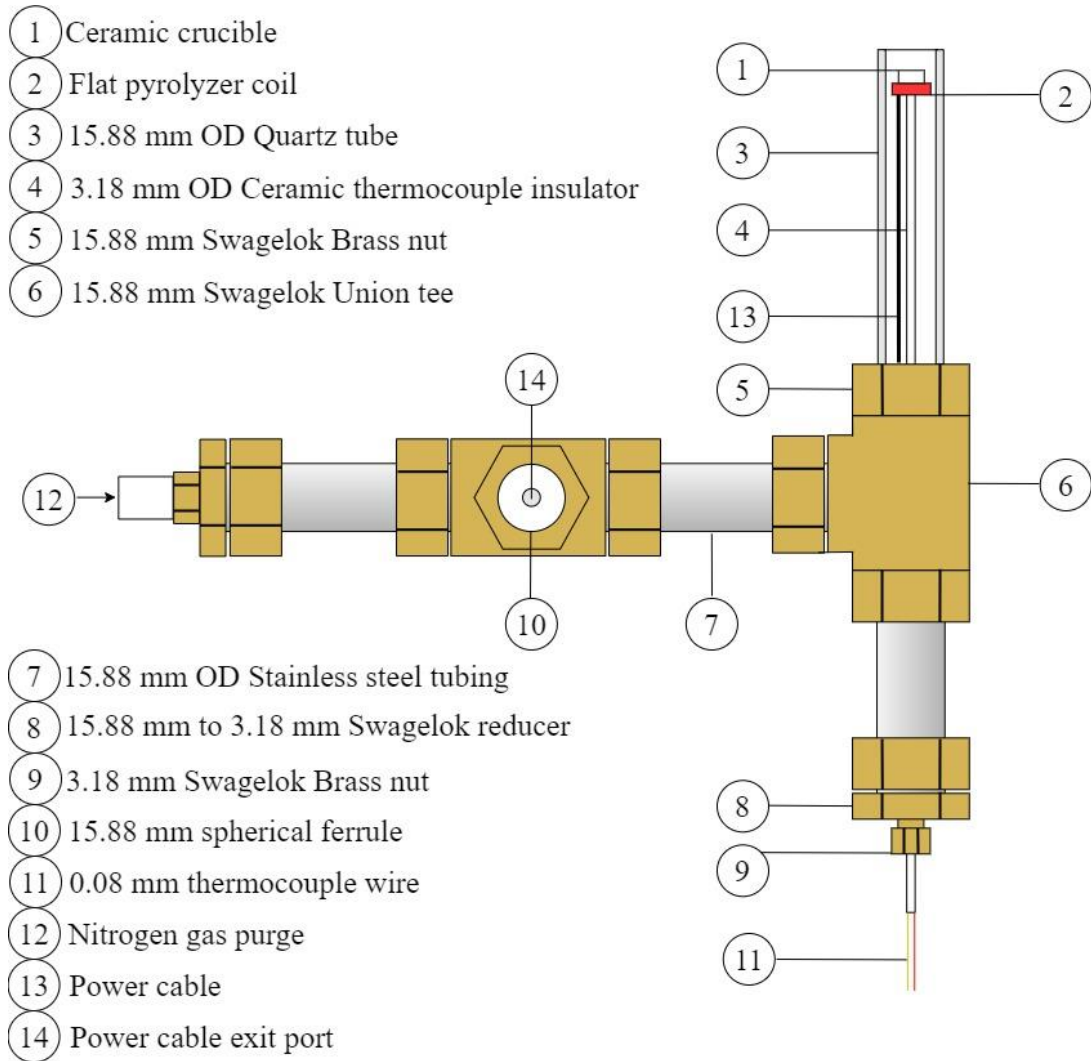


Figure 2.3: Schematic diagram of the flat pyrolyzer coil/thermocouple system which will replace the Pyroprobe pyrolyzer

## 2.2 Power Supply

The flat radial pyrolyzer heating coil was powered with the use of a Cotek 800 W switching mode power supply. The power supply has a programmable output voltage ranging from 0% to 105% with a maximum output voltage of 36 V. This specific power supply was selected as it provides the user with a constant voltage output with a sensitive voltage range. This is important due to the low resistance of the pyrolyzer coil, 0.6 ohm. The low resistance of the coil results in large amperage readings for low voltage input values. The power supply was selected such to more closely approximate the heating conditions of a sample during cone calorimetry experiments. During a cone calorimetry experiment, the sample is exposed to the prescribed heat flux as soon as the sample is mounted below the conical heater, resulting in the sample surface temperature nearly instantaneously equaling the temperature of the conical heater. This idealized behavior is similar to a unit step function as depicted per Figure 2.4. The MCC temperature profile is linear with time. The power supply for the new MFC pyrolyzer coil was selected to more closely approximate the temperature profile of the cone calorimeter and to avoid the linear heating behavior of an MCC test. The constant input voltage to the power supply was considered to emulate the constant heat flux exposure of a sample during cone calorimetry experiments. The MFC pyrolyzer coil temperature profile is depicted per Figure 2.4.



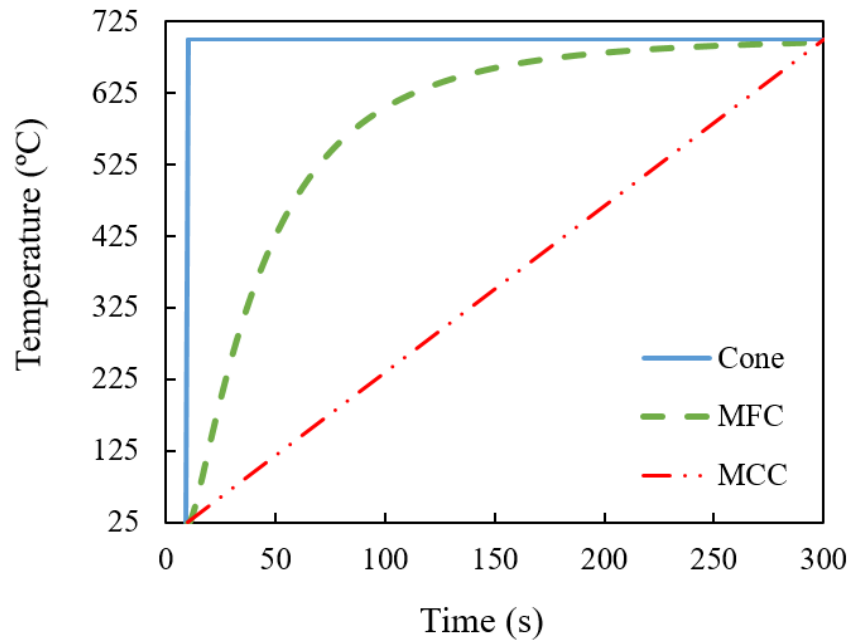


Figure 2.4: Idealized surface temperature profiles for cone calorimetry, MFC and MCC experiments

The input voltage (on the control end of the power supply) at which mechanical failure of the pyrolyzer coil took place was determined to ensure that allowable user input voltage to the power supply was not exceeded during a test. It was noted that for a pyrolyzer coil having a resistance of approximately 0.6 ohm, an input voltage of 1.2 V to the power supply and a subsequent output voltage of 6.1 V to the pyrolyzer coil would result in the mechanical failure of the coil at 62.42 W. During normal operation, the pyrolyzer coil was supplied with an output voltage of 4.3 V, resulting in a constant power of 30.8 W to ensure that a measured end temperature in excess of 695 °C was obtained. The nitrogen purge flowrate was optimized considering this end temperature for the pyrolyzer coil.

### 2.3 Nitrogen flowrate optimization

A nitrogen purge stream is introduced upstream of the pyrolyzer coil that is housed within a 15.8 mm outer diameter quartz tube. This purge gas flows past the lip of the ceramic crucible holding the sample and aids in the transport of the pyrolyzate gases upward toward the hot wire igniter. The flowrate of the nitrogen purge is an important parameter that was optimized to ensure the correct operation of the MFC. The purge gas flowrate was optimized to ensure that the flowrate was large enough to guarantee non-oxidative pyrolysis at the surface of the sample as well as to minimize the dilution effect of the purge gas when transporting the pyrolyzate gases toward the igniter. The purge gas flowrate was also optimized to minimize the deposition of volatiles on the inner surface of the quartz tube, as this would result in fuel not being delivered to the flame, and a subsequent error in the measurements.

The original strategy was to reduce the nitrogen flowrate from the original flowrate of 100 SCCM, calculated at 25 °C and 101.325 kPa, in order to reduce the dilution effect of the purge gas. The production of air-borne particulates and the subsequent deposition of these particulates along with the condensation of volatile gases onto the interior wall of the quartz tube, which houses the pyrolyzer coil, was documented. It was used as a measure to determine the efficiency of the purge gas stream to carry pyrolyzate gases and particulates upwards past the lip of the quartz tube. The deposition of gaseous pyrolyzates and airborne particulates is not favorable as this impacts the calculated heat of combustion of the burning material and alters the expected purge gas flow profile flowing past the exterior walls and lip of the crucible. This altered flow

could compromise the expected concentration of pyrolyzate gases transported to the hot wire igniter. This in turn compromises the ignition time and a subsequent reduction in the HRR of the burning material due to a shorter burn time. The flowrate optimization was performed using high-density polyethylene (HDPE), a material known to produce high molecular weight compounds which can condense..

The sample masses for the HDPE used during this test were approximately 35 mg, with the only varying parameter being the purge flow rate. The test was conducted to calculate the mass of pyrolyzates that had been deposited on the interior walls of the quartz tube housing using a pyrolyzer coil power equal to 30.8 W. This was done by noting the mass of the quartz tube prior to the start and at the end of each test. As per Figure 2.5, it is noted that the deposition mass of pyrolyzates decreases as the purge flowrate increases.

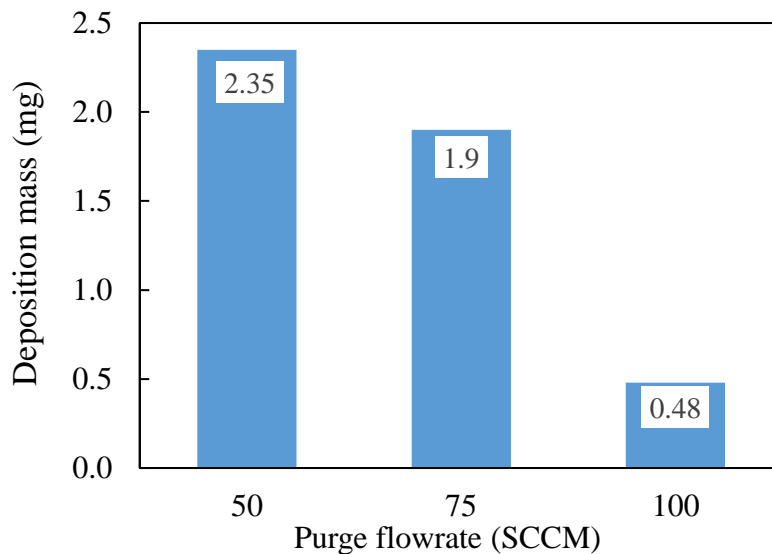


Figure 2.5: Pyrolyzate gases and airborne particulate condensation mass as a function of the purge gas flowrate with the pyrolyzer coil set at 30.8 W

The purge gas flowrate was also noted to have a strong influence on the ignition probability of the material, as the flowrate was indicative of the amount of pyrolyzate gases that would be carried towards the hot wire igniter without condensing on the interior wall of the quartz tube housing the pyrolyzer coil system. During the normal operation of the MFC, a gauge back-pressure within the combustor in the range of 0.5 to 0.75 psi is typical, potentially reducing the rate at which pyrolyzate gases are transported toward the hot-wire igniter. The selected flowrate of 100 SCCM was, however, sufficient and flaming ignition for all material samples was expected.

The selected nitrogen flowrate also ensured that the axisymmetric diffusion flame developed at the lip of the quartz tube and not at the lip of the crucible. The development of the flame at the lip of the crucible is not a favorable condition. This is indicative of oxygen present at the crucible lip prior to ignition of the pyrolyzate gases – potentially resulting in the oxidative pyrolysis at the top surface of the sample prior to ignition. The other reason for this unfavorable operating condition is that the heat of the flame is fed back to the surface of the sample. This flame heat feedback could result in the heat transfer from the pyrolyzer coil to the bottom surface of the sample no longer dominating the pyrolysis of the sample. The required flaming combustion condition is depicted per Figure 2.6 where the flame is present at the lip of the quartz tube housing the pyrolyzer coil and not at the lip of the ceramic crucible.



Figure 2.6: MFC test with the axisymmetric diffusion flame present at the required position i.e. the lip of the crucible housing the pyrolyzer coil

#### 2.4 *MFC Instrumentation Layout*

The MFC instrumentation setup was similar to that of the work done by Raffan-Montoya et al. [19] with the major difference being the new pyrolyzer system. The instrumentation layout of the newly designed MFC is presented per Figure 2.7 and consists of four different parts: the pyrolyzer system, the combustor, the gas analyzer system and the control panel. All MFC experiments were conducted using ceramic crucibles without lids. Lids were not used for any of the experiments to facilitate the ignition of the pyrolyzate gases and to ensure that these gases were more readily carried to the lip of the quartz tube housing the pyrolyzer coil via the nitrogen purge. The pyrolyzate gases, swept up by the purge flow, meet the co-flow gas at the lip of the quartz tube housing the pyrolyzer coil and are subsequently ignited by a hot wire igniter operated at 50 W. The co-flow gas could be air or a user-defined mixture of high-purity

nitrogen and ultra-high-purity oxygen gas. The flowrates of both the purge and co-flow gas were both controlled with the use of component-specific low pressure drop mass flowmeters (Alicat Whisper MW series). The base of the combustor comprised the use of a circular perforated brass sheet and 3 mm diameter glass beads that would ensure a homogenized co-flow. This delivery guarantees a low-speed co-flow of gas with minimal radial gradients, simulating the semi-quiescent conditions typical of the early stages of a developing fire.

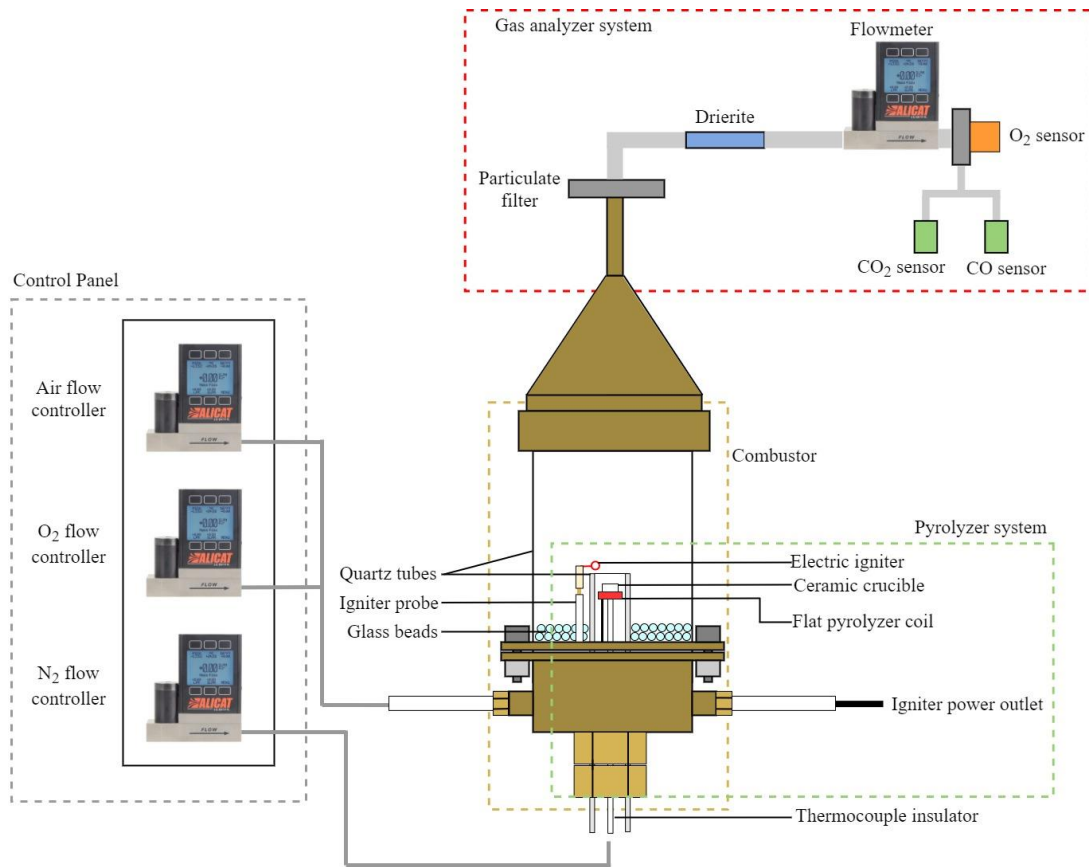


Figure 2.7: Schematic diagram of the new MFC instrumentation layout

The combustion chamber comprised a 75 mm outer diameter, low thermal expansion coefficient quartz tube with said quartz tube having a height of 127 mm. The quartz tube is transparent which allows for direct measurement of the flame height and time-to-ignition data of a sample via video. The base of the combustion chamber consists of a brass cylinder with an 89 mm outer diameter and a height of 48.3 mm. The function of the base was to ensure a homogenized co-flow, to connect the pyrolyzer system to the combustion chamber and to introduce the hot wire igniter to the system [28]. The products of combustion travel upward, away from the flame, through a conical hood that collects and accelerates the flow toward the gas analyzing system. The angle of the hood was chosen to minimize the pressures losses in the system while accelerating the flow, thereby reducing the delay time between the flaming combustion process and detection of the process by the gas analyzers [28].

After the combustion products travel past the hood, all solid particulates are retained in a Whatman GMF 150 2  $\mu\text{m}$  glass microfiber filter which has been chosen to avoid flow obstructions, even for highly sooting materials. The remaining gaseous products are scrubbed to remove  $\text{H}_2\text{O}$  and then enter the gas analyzer section where the outlet flowrate and  $\text{O}_2$  concentration are simultaneously measured. The  $\text{O}_2$  concentration is measured with a fuel-cell type automotive oxygen sensor (Teledyne R17-a) which measures the volumetric fraction of  $\text{O}_2$  in the gas stream. The  $\text{CO}_2$  and  $\text{CO}$  concentrations are measured downstream of the  $\text{O}_2$  sensor using infrared sensors (Gascard, Edinburgh Sensors) having a range of 0 – 10 %. The exhaust stream is then vented to an ambient pressure environment.

The K-type, 0.08 mm bead diameter, thermocouple used to measure the surface temperature of the sample was wired to a National Instruments analog voltage output module (NI-9263). It was added to the DAQ already connecting the O<sub>2</sub>, CO<sub>2</sub> and CO sensors as well the flowmeter downstream of the combustion chamber. The devices were sampled digitally at 4 Hz to collect the test data using the above-mentioned National Instruments hardware and relevant software (LabView).

### 2.5 *Analysis of Power and Temperature Relationship*

The relationship between the measured temperature of the pyrolyzer coil and the user-defined input voltage to the power supply was considered. The two voltage inputs to the power supply that were used for each test were selected to correspond to a conditioning and heating ramp. The input voltages to the power supply corresponded to a pyrolyzer coil power of 0.56 W for the first heating ramp (conditioning ramp) and 30.8 W for the second heating ramp. The temperature profiles were obtained using a fully assembled, pressurized MFC setup with the correct co-flows and an empty ceramic crucible as depicted per Figure 2.8. The reproducibility of the temperature profile for each input voltage to the power supply was considered.



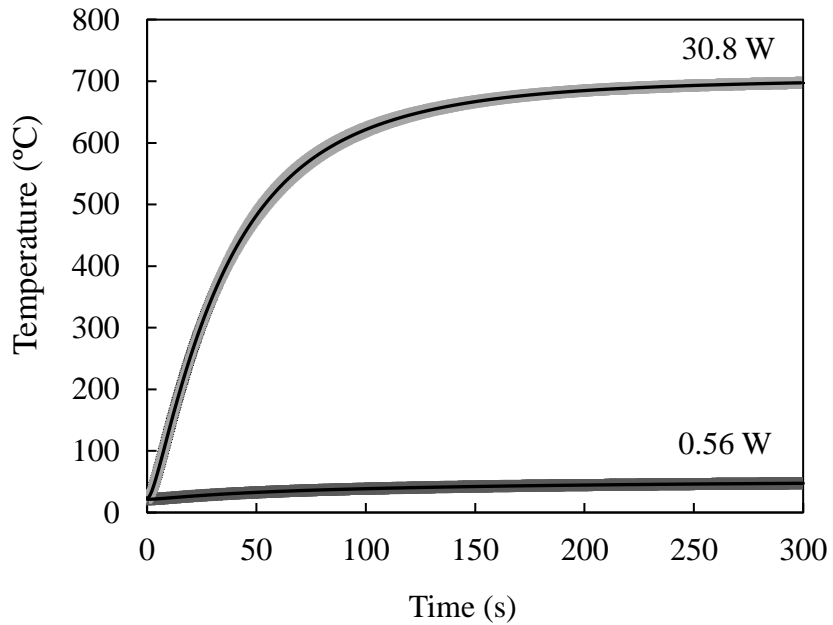


Figure 2.8: Temperatures profiles each with its corresponding coil power which was used during the operation of the MFC

The maximum heating rate for the heating ramp was calculated to be equal to  $13.4\text{ }^{\circ}\text{C}\cdot\text{s}^{-1}$  as depicted per Figure 2.9. This is much higher than that used in the MCC i.e.  $1\text{ }^{\circ}\text{C}\text{ s}^{-1}$ . This was a favorable condition as this high heating rate is more representative of a real fire scenario.

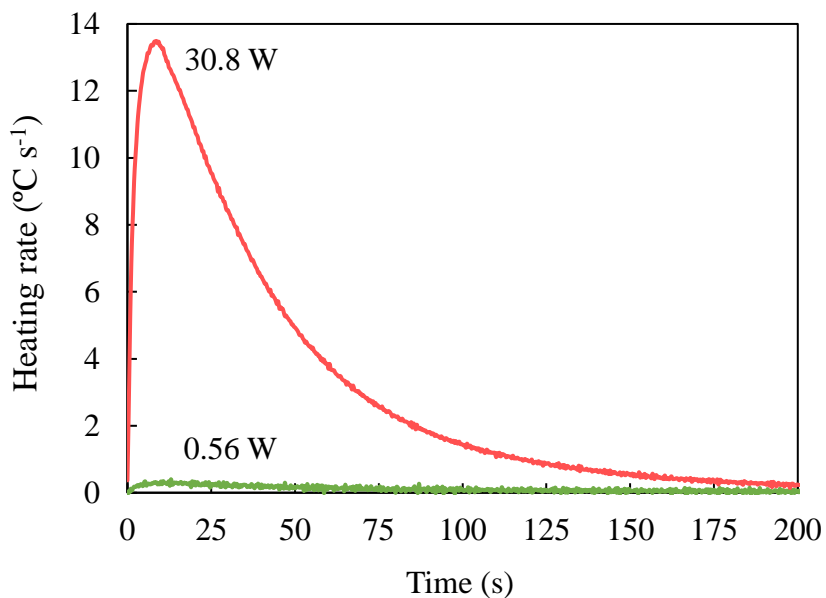


Figure 2.9: Heating rate profiles for each with its corresponding coil power

## 2.6 *Heating Ramps*

The coil heating program consisted of an initial 180-second conditioning temperature ramp up to an equilibrium temperature of approximately  $43.7 \pm 0.1$  °C with the corresponding electric power of the pyrolyzer coil at 0.56 W. This is followed by a 210-second heating temperature ramp up to an equilibrium temperature of approximately  $695.1 \pm 0.3$  °C (electric power at 30.8 W), as depicted per Figure 2.10.

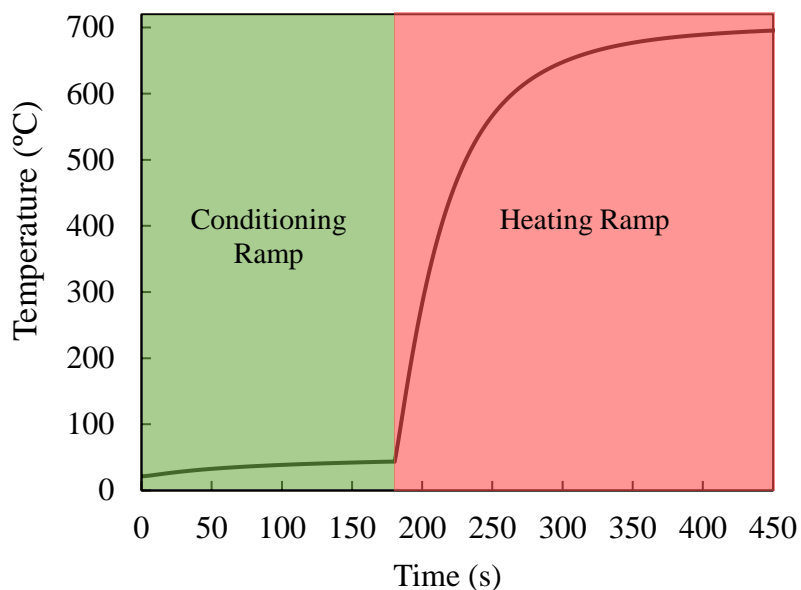


Figure 2.10: Coil heating program highlighting both the Conditioning and Heating ramp used during an MFC experiment

The hot wire igniter was not turned on prior to the start of the heating ramp as the radiant heat from the igniter would start melting the top surface of the sample. The effect of the hot wire igniter being the dominant heating mechanism of the sample was minimized by only turning on the igniter after the heating ramp was initiated. The heating rate of the pyrolyzer coil would then be much larger than that of the igniter coil.

The idealized radiant heat flux from the surface of the pyrolyzer coil was calculated using Equation (7 with  $\epsilon$  being the emissivity of the pyrolyzer coil assembly, which was assumed to be equal to 1.0,  $\sigma$  the Stefan-Boltzmann constant equal to  $5.67 \times 10^{-8} \text{ W m}^{-2} \text{ K}^{-4}$  and  $T_{\text{rad}}$ , K, equal to the maximum equilibrium temperature. The pyrolyzer coil was assumed a black body for ease of calculation and was only used to analytically approximate the idealized radiant heat flux. The maximum heat flux from

the surface of the pyrolyzer coil was calculated to be equal to 49.8 kW/m<sup>2</sup> considering the end temperature of the heating ramp (695.1 ± 0.3 °C).

$$Q = \varepsilon\sigma T_{rad}^4 \quad (7)$$

### 2.7 Pyrolyzer Coil Reproducibility

The same pyrolyzer coil was used to conduct all the MFC experiments. More than 40 experiments at the maximum input voltage to the power supply were conducted. The reproducibility of the temperature profiles was tested considering the use of two different pyrolyzer coils. The measured end temperature of each of the pyrolyzer coils at a specified electric power was compared when tested in the presence of a nitrogen purge flowrate of 100 SCCM as per Figure 2.11. It was noted that the different coils are reproducible when built considering the guidelines as highlighted in Section 2.1.

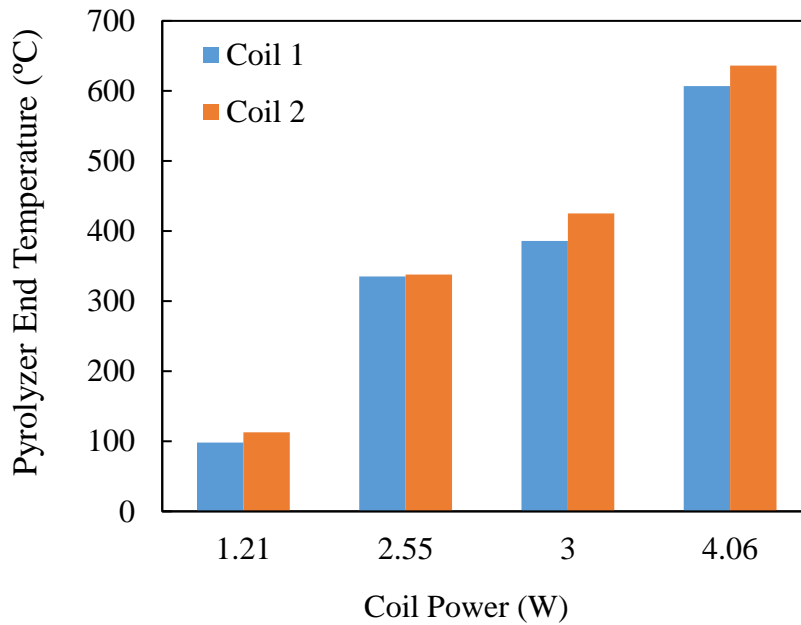


Figure 2.11: Relation between the measured end temperature and the user-defined input voltage to the power supply using a co-flow of 100 SCCM N<sub>2</sub>

## 2.8 Temperature Calibration

The calibration of the K-type thermocouple was done considering the known melting temperatures of four metals: aluminum, indium, zinc, and lead. The calibration compensated for the thermal lag between the sample surface touching the bottom interior of the ceramic crucible and the thermocouple in contact with the bottom exterior surface of the ceramic crucible. The melt temperature of the metals as measured by the thermocouple was plotted against the known melting temperature of each of the four metals, as per Figure 2.12.

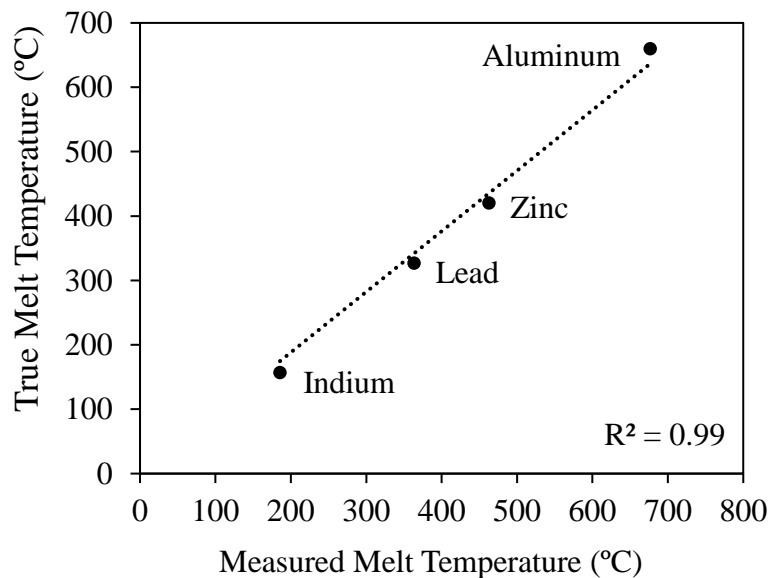


Figure 2.12: Calibration curve used to compensate for the thermal lag present between the thermocouple bead and the bottom surface of the sample within the ceramic crucible

## 2.9 MFC Processing Script

The MATLAB script that was previously developed for the post-processing of data gathered from the MFC was revised for the use of a new pyrolyzer coil heating program. The baseline readings are obtained at two separate time intervals where the system is assumed to be operating under steady conditions. The baseline readings were used to determine the oxygen concentration and mass flowrate of the system at these two intervals. The temperature profiles indicating where the two baselines were selected is depicted per Figure 2.13. The start of the test ( $t = 0$  s) is coincident with the start of the first heating ramp i.e. the Conditioning ramp. The first baseline is obtained during the Conditioning ramp, between 150 and 170 seconds after the initiation of the test. The second baseline is obtained between 410 and 430 seconds after the initiation of the test during which time the pyrolyzer coil temperature had reached an approximately equilibrium end temperature. These baselines were always selected at the same time intervals and were the same for each experiment.

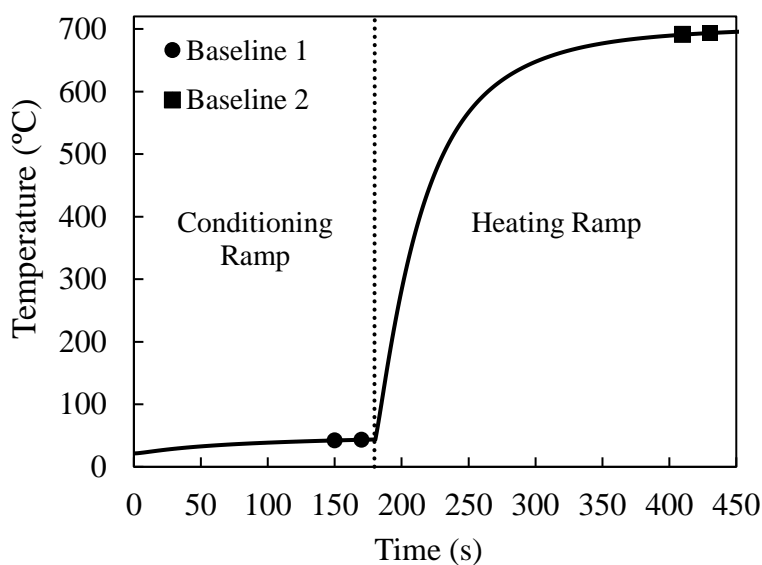


Figure 2.13: Baseline measurement times considering temperature profile of a representative MFC experiment

Both baselines are averaged over 20 seconds, with the first baseline ending 10 seconds before the end of the Conditioning ramp and the second baseline ending 20 seconds before the end of the Heating ramp. Any sensor drift is compensated by use of linear interpolation with time between the two baseline readings. This also allows for the determination of the inlet volumetric flowrate and oxygen concentration, which corresponds to the averages of these quantities taken during the first baseline calculation.

#### 2.10 *Summary of Pyrolyzer development*

A circular ceramic test tube with an outer diameter of 8 mm and a height of 4.5 mm will replace the quartz test tube used in the previous MFC setup. This will allow for the testing of both granular and disk-like plates, with the plates replicating that of the samples prepared for cone calorimeter tests. The size of the circular ceramic crucible allows for the testing of charring materials without the clogging of the crucible during the test.

The flaming combustion of the sample represented by an axisymmetric diffusion flame will be maintained while the addition of a calibrated type K thermocouple will enable the direct measurement of the sample temperature during the test. The thermocouple will be in contact with the bottom exterior of the ceramic crucible and mounted through a central hole of the ceramic housing of the pyrolyzer coil. The

pyrolyzer coil will be designed in-house and will comprise the use of 0.4 mm thick square nickel-chrome wire. The shape of the pyrolyzer will be changed from the spiral configuration of the pyroprobe pyrolyzer to a flat radial configuration. This will significantly improve the cost of the pyrolyzer all while more accurately replicating the one-dimensional heating of a sample as in the cone calorimeter.



### 3 Chapter 3: Experimental Methodology

#### 3.1 Material Specification, Preparation, and Test Matrix

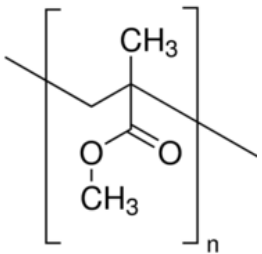

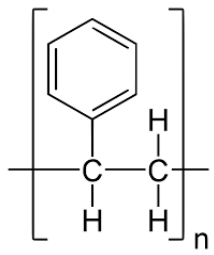

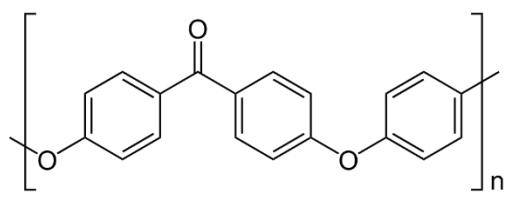

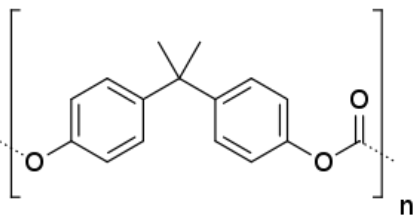

The five materials that were used during this study include Poly (methyl methacrylate) (PMMA), High-Impact Polystyrene (HIPS), Poly (ether ether ketone) (PEEK), Bisphenol-A Polycarbonate (PC), and rigid Poly (vinyl chloride) (PVC). These materials were selected to be representative of a wide range of synthetic polymers with distinct combustion properties. PMMA is representative of a material that undergoes a near complete combustion process; HIPS, a material with high sooting propensity when burning; PEEK and PC, materials that decomposes at a high temperatures while forming an intumescent char as part of its combustion process; and PVC, a material that produces halogenated products that are known to retard the combustion process in the gas-phase.. Table 3.1 and Table 3.2 provides additional information about the materials that were used during this study.

Table 3.1: Materials studied in this work.

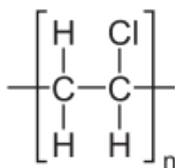
Polymer	Trade Name	Manufacturer	Thickness (mm)	Color
PMMA	Acrylite	Evonik Industries	2.92	Clear
HIPS	HIPS	Spartech Plastics	2.97	White
PEEK	PEEK 450 G	Victrex plc	3.18	Dark Yellow

PC	Makrolon GP	Bayer	2.97	White
PVC	Vintec I	Vycom Plastics	3.10	Dark Grey

Table 3.2: Chemical structure of studied materials.

Polymer	Repeat Unit	Test sample
PMMA		
HIPS		
PEEK		
PC		

PVC



The test matrix that shows all the experiments that were conducted for each material using cone calorimetry, MCC, or MFC is depicted per Table 3.3. The heat flux that was used for the cone calorimetry experiments was equal to  $50 \text{ kW}\cdot\text{m}^{-2}$ . A heating rate of  $1 \text{ }^\circ\text{C}\cdot\text{s}^{-1}$  was used during MCC experiments, and a pyrolyzer coil maximum heat flux of  $50 \text{ kW}\cdot\text{m}^{-2}$  was used for all MFC experiments.

Table 3.3: Test matrix for cone calorimetry, MCC, and MFC experiments

Material	Experiment type	Number of experiments
PMMA	Cone calorimetry	2
	MCC	3
	MFC	4
HIPS	Cone calorimetry	2
	MCC	3
	MFC	4
PEEK	Cone calorimetry	2
	MCC	3
	MFC	4
PC	Cone calorimetry	2

	MCC	3
	MFC	4
	Cone calorimetry	2
PVC	MCC	3
	MFC	4

### 3.1.1 Cone Calorimetry Sample preparation

The samples that were prepared for the cone calorimetry experiments were each 100 mm  $\pm$  2 mm squares with a thickness of 2.94 mm  $\pm$  0.1 mm. The mass and thickness of each sample material is presented per Table 3.4. Prior to testing, the samples were conditioned in a desiccator for at least 24 hours. The sample was weighed and a 0.025 mm-thick piece of heavy-duty aluminum foil was wrapped around the sample, such that only the top surface of the sample was exposed. A retainer was used and reduced the exposed surface area of the sample from 0.1 m<sup>2</sup> to 0.088 m<sup>2</sup>. The aluminum foil covering the sides of the sample was raised an additional 2 mm from the top surface of the retainer to minimize the potential of the pyrolyzing sample spilling out of the aluminum foil casing or onto the top surface of the retainer. The bottom surface of the sample was glued onto the interior of the aluminum foil casing using 2.4 g of Loctite clear epoxy. The bottom surface of the aluminum foil was then glued onto a 6.35 mm thick Kaowool ceramic fiber board which was subsequently stacked on top of two additional pieces of 6.35 mm thick fiberboard. Both the retainer and the epoxy were used to minimize the warping effect of the sample during the test.

Table 3.4: Average sample mass and thickness used for the cone calorimeter experiments

Material	Sample mass (g)	Sample thickness (mm)
PMMA	$34.2 \pm 0.3$	$2.8 \pm 0.08$
HIPS	$31.0 \pm 0.09$	$3.0 \pm 0.08$
PEEK	$41.8 \pm 1.0$	$3.0 \pm 0.08$
PC	$36.2 \pm 0.2$	$2.83 \pm 0.09$
PVC	$43.1 \pm 0.1$	$3.05 \pm 0.13$

### 3.1.2 *Microscale Combustion Calorimetry Sample Preparation*

All samples prepared for the MCC experiments had masses ranging from 3.95 – 5.15 mg as depicted per Table 3.5. Two distinct sample geometries were used during the MCC tests: granulated powders or solid shavings. The powders were prepared by manually filing the sheet using a second cut mill flat file. The shavings were prepared with the use of a band saw. The shavings were prepared such that they would easily fit into the crucible to ensure proper thermal contact between the sample and the bottom interior surface of the crucible. Two different sample geometries were considered to determine whether the powders samples or the sample shavings more adequately capture the burning behavior of a material.

Table 3.5: Average sample mass for the MCC experiments

Material	Granulated powder sample mass (mg)	Sample shaving mass (mg)
PMMA	$3.95 \pm 0.08$	3.74
HIPS	$3.76 \pm 0.02$	3.77
PEEK	$4.42 \pm 0.2$	5.06
PC	$4.34 \pm 0.09$	5.09
PVC	$4.5 \pm 0.06$	5.15

### 3.1.3 Milligram-scale Flame Calorimetry Sample Preparation

Samples prepared for MFC experiments also consisted of two distinct geometries: granulated powders and disk-like plates. Two different sample geometries were considered to evaluate whether either the granulated powders or the disk-like plates more accurately emulate the burning behavior of samples as seen during cone calorimetry experiments. Multiple tests were conducted to determine the sample mass for each material that would conform to the requirements of the system regarding the size and shape of the sample. The granulated powder samples were prepared using the same methodology as for the MCC samples, having a mass of  $35.33 \pm 0.46$  mg. The disk-like samples were prepared using a 7 mm diameter hole punch which would ensure a more reproducible sample shape and size as depicted per Figure 3.1. The mass for both sample geometries and the thickness of the disk-like plates are presented in Table 3.6. The preparation technique used to prepare the disk-like samples ensured that the maximum contact area between the sample and the bottom interior of the crucible was

obtained. This would aid to better detect any sudden temperature variations at the bottom surface of the sample during the pyrolysis thereof. The diameters of the material samples were subsequently reduced with the use of grit aluminum oxide sandpaper until the required sample mass was obtained.

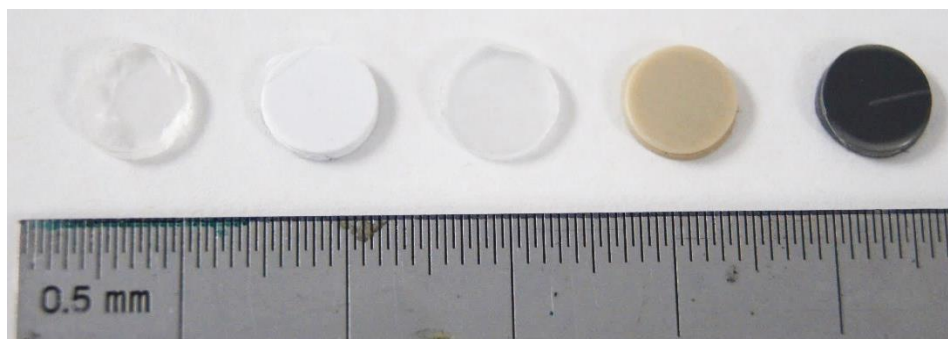


Figure 3.1: Disk-like plates produced with the use of a 7 mm diameter hole punch. The samples from left to right are: PMMA, HIPS, PC, PEEK, and PVC

The mass of the disk-like plates was selected to ensure that any of the sample did not spill out of the crucible during the test, but also to ensure that a peak oxygen concentration decrease of 5 % was not exceeded. It was noted that for the intumescent chars, the tendency of the sample to spill out of the crucible during a test increased as the sample mass of the intumescent-charring material increased. The sample mass was reduced such that the effect of sample spilling was eliminated – but it was also only reduced to such an extent to ensure that ignition of the pyrolyzate gases was still possible. Sample masses for materials such as PMMA and HIPS were increased to a mass just larger than the granulated powder sample masses while still adhering to the contact area and peak oxygen consumption concentration criteria. The sample masses

of the intumescent and charring materials were increased to an upper limit of 60 mg. The sample mass of PC was reduced to a mass lower than the mass used for the granulated powder samples. This was done because the PC samples tended to spill out of the crucible during an experiment. Table 3.6 presents the sample masses that were used for each of the materials in the MFC.

Table 3.6: Average mass for granulated powder and disk-like plate samples prepared for MFC experiments

Material	Granulated powder (mg)	Disk like plate (mg)	Sample thickness (mm)
PMMA	$34.51 \pm 0.66$	$40.37 \pm 0.17$	$1.17 \pm 0.026$
HIPS	$35.31 \pm 0.5$	$38.89 \pm 0.25$	$1.29 \pm 0.051$
PEEK	$35.35 \pm 0.55$	$55.39 \pm 1.3$	$1.35 \pm 0.10$
PC	$35.75 \pm 0.62$	$33.78 \pm 1.4$	$1.10 \pm 0.064$
PVC	$35.9 \pm 0.62$	$57.08 \pm 2.0$	$1.37 \pm 0.026$

The variation in sample masses for each of the materials is much larger than that of the variation in sample masses for the granulated powder materials. It should, however, be noted that a larger sample mass is beneficial as this increases the likelihood of ignition of the pyrolyzate gases. A larger sample mass, with a near constant thickness, allows for a larger contact area between the sample and the crucible.



### 3.2 Cone Calorimetry Experimental Methodology

Experiments using cone calorimetry were conducted in accordance with ASTM E1354 to collect data pertaining to the HRR, MLR and smoke production of a burning material. The data pertaining to the MLR of a test sample was obtained using a Sartorius component weight unit with a 0.01 g resolution, with the sample mass data obtained at a frequency of 10 Hz. The HRR was calculated considering the oxygen consumption principle with the oxygen concentration measured using a paramagnetic oxygen sensor. The data was obtained at a frequency of 0.5 Hz,

The smoke obscuration measuring system is comprised of a JDSU 1108P helium neon laser with a wavelength of 632.8 nm and a power of 0.5 mW. The laser beam is split into two separate paths, with one of the beams directly entering the reference photodiode and the other beam traveling through the duct (and smoke if present) before reaching the measuring photodiode. The voltage of each photodiode is directly measured and subsequently used for signal processing and calibration. The laser was calibrated with the use of multiple neutral density filters with optical densities ranging from 0.1 to 2.5. Optical density is a measure of the fraction of light that is transmitted through the filter as depicted Table 3.7 [29]. The neutral density filters block light and the measurement photodiode voltage decreases as the optical density of each filter increases (representative of different smoke densities in the exhaust duct). The zero-value extinction coefficient was subsequently verified prior to the commencement of each day of experiments in the cone calorimeter. The ratio of the

voltages of both the measurement and reference photodiode was related to the optical density of the filters, which in turn can be related to the smoke density [23].

Table 3.7: Optical density as a function of the fraction of light transmitted

Optical density	Fraction of light transmitted
0.1	0.8
0.3	0.5
0.6	0.25
0.9	0.13
2.5	0.032

Before the commencement of the experiments, all filters, Drierite, and Ascarite on the cone calorimeter was checked and replaced as needed. The O-ring from the smoke particulate filter was cleaned daily as well as after testing a highly sooty material. The gas analyzers, load cell, laser diagnostic, and methane calibrations were performed daily. A water-cooled Schmidt-Boelter heat flux gauge mounted 25 mm from the bottom surface of the conical heater was used to measure the incident heat flux of the radiant coil heater as a function of the measured temperature of the heater. After the calculation of the calibration factor, a baseline test was conducted using a 6.35 mm-thick black PMMA plate. The heat flux that was used for all the experiments was  $50.85 \pm 0.52 \text{ kW/m}^2$ . The HOC of the black PMMA plate was then evaluated and compared to the standard value of 25 kJ/g to confirm that the cone calorimeter was properly calibrated. The sample was mounted 25 mm below the bottom surface of the conical

heater with the use of a sample holder assembly which was mounted on top of a Sartorius component weigh unit.

Flaming ignition was obtained using a spark igniter that was placed in between the top face of the sample and the conical heater. The spark igniter was switched on directly after the sample was mounted beneath the conical heater and removed from this position after self-sustained flaming combustion was visually verified. The samples were left to burn until extinguishment of the sample was obtained, which was indicated by the absence of visible flames above the surface of the material. The times that were documented during the test are as follows: the placement of the sample onto the sample holder, the time to ignition, the extinguishment of large self-sustaining flames on the surface of the char formed by PC, PEEK and PVC or the absence of a flame for the non-charring materials, and the extinguishment of the flame at the surface of the sample. The mass of the aluminum foil and any remaining solid residue was measured for the purpose of calculating the char yield of the sample.

### 3.3 *MCC Experimental Methodology*

MCC [11] is a standardized milligram-scale test that is used to calculate the HOC of pyrolyzate gases produced from the anaerobic, thermal decomposition of a sample. A schematic representation of the MCC is depicted as per Figure 3.2. The calculated HOC of the pyrolyzate gases provides a relationship between the gas-phase and condensed-phase phenomena. The MCC provides the user with the HRR as a function of the temperature of the sample, as well as the duration of the test. All samples were

prepared prior to testing and were left in a desiccator chamber for at least 24 hours. The mass of each sample material was measured using a laboratory microbalance (A&D Weighing, BM-22) with a 0.001 mg resolution

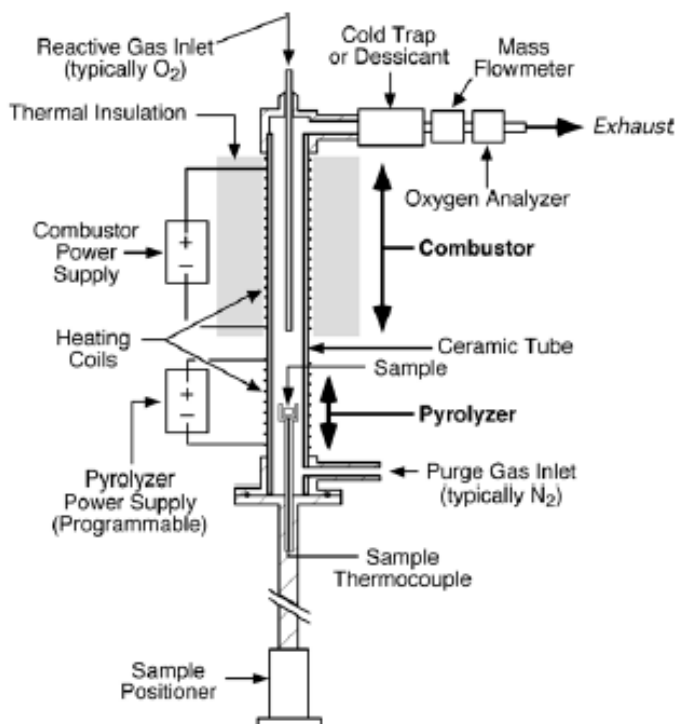


Figure 3.2: Schematic layout of the MCC instrumentation

The MCC experiments were conducted such that the pyrolyzer was linearly heated at a rate of  $1\text{ }^{\circ}\text{C s}^{-1}$  up to  $750\text{ }^{\circ}\text{C}$  with the combustor temperature being set to  $900\text{ }^{\circ}\text{C}$ . The combustor was set to this temperature to ensure that all the pyrolyzate gases were completely oxidized. The sample was heated within the pyrolyzer region of the MCC in a completely anaerobic environment. The anaerobic environment was maintained with the use of a nitrogen purge flow of 80 SCCM. The formed pyrolyzate

gases are then mixed with excess oxygen, at a flowrate of 20 SCCM, in the combustor zone of the MCC.

All MCC experiments were conducted using small ceramic crucibles without lids. Lids were not used for any of the experiments, as this ensured that the pyrolyzate gases were readily carried into the combustor via the nitrogen purge. All MCC tests were conducted with a prescribed temperature program with the initial stage having a conditioning period where the sample temperature was kept at a temperature of 75 °C. It was determined that PEEK was the material that decomposed at the highest temperature but had fully decomposed at a temperature lower than 750 °C.

The MCC was fully calibrated approximately four times a year, with, at least, the oxygen sensor calibrated daily when used. The O<sub>2</sub> sensor was calibrated using two data points. The sensor was first zeroed by flowing N<sub>2</sub> gas through the system. The second reference point was obtained by using a mixture of 20.1 vol% O<sub>2</sub>.

The thermocouple was calibrated based on the known melting temperatures of a range of pure metals to ensure accurate sample temperature measurements as described per ASTM D7309. The thermocouple calibration compensated for the thermal lag between the sample surface touching the bottom interior of the crucible and the thermocouple located on the bottom exterior of the crucible. The metals that are used for this calibration are aluminum, indium, zinc and lead.

The oxygen sensor was calibrated using a pre-defined oxygen/nitrogen mixture to obtain accurate oxygen consumption measurements, which in turn is directly related

to the heat release rate of the volatile pyrolyzate. A baseline test using general purpose polystyrene was performed at the beginning of each testing day to quantitatively verify the calibration of the instrument. The goal of this baseline test was to obtain a normalized complete HOC value (by initial sample mass) of approximately  $40.2 \pm 0.6$  kJ/g [11]. Once it was confirmed that the calibration had been successfully performed, the sample was loaded onto the platform housing the thermocouple where after the heating program was initiated. The char yield for each sample was then measured once the pyrolyzer had cooled down to temperature lower than 75 °C.

#### 3.4 MFC Experimental Methodology

Experiments using the MFC were conducted to collect data pertaining to the HRR, ignition temperature, time to ignition, char yield, and air-borne particulate yield of a material. The HRR of a material was obtained considering the oxygen consumption principle and measuring the O<sub>2</sub>, CO<sub>2</sub> and CO concentrations. The oxygen concentration was measured using a fuel-cell type automated oxygen sensor, and infrared sensors were used to measure both the carbon monoxide and carbon dioxide concentration. The surface temperature of the sample was measured using a K-type 0.08 mm bead diameter thermocouple.

The calibration procedure for the MFC included the daily calibration of the O<sub>2</sub>, CO<sub>2</sub> and CO sensor, as well as the bi-monthly calibration of the mass flowmeter downstream of the combustor and the K-type thermocouple. The O<sub>2</sub> sensor as well as the CO<sub>2</sub> and CO sensors were calibrated using two data points as the sensors have a

linear output. All three sensors were first zeroed by flowing N<sub>2</sub> gas through the system. The second reference point was obtained by first using a mixture of 20.1 vol% O<sub>2</sub> for the O<sub>2</sub> sensor and secondly, a custom mixture containing 4 vol% CO<sub>2</sub> and 0.4 vol% CO for the other two sensors.

The mass flowmeter was calibrated using a MesaLabs Defender 530 flow calibrator. The mass flowmeter was calibrated using compressed air in the range of 3.5 SLPM and 4.5 SLPM with the expected system flowrate equal to 4 SLPM. The Drierite used to scrub water downstream of the mass flowmeter was replaced daily.

The mass of each sample material was measured using a laboratory microbalance (A&D Weighing, BM-22) with a 0.001 mg resolution. The initial mass of the sample and ceramic crucible, as well as the initial mass of the particulate filter, was noted. These values would later be used to calculate the char and particulate yield of a sample. The ceramic crucible was then placed on top of the pyrolyzer coil with the new particulate filter added upstream of the combustor. The purge flowrate was set at 100 SCCM using the mass flow controller upstream of the combustor with the air co flow being selected such that the total measured flowrate downstream of the combustor was equal to 4 SLPM. The combustor hood was then sealed in place and a leak test was conducted using 4 SLPM of co-flow air. A gradual decrease of the measured downstream flowrate or a backpressure lower than 0.5 psi was indicative of a leak in the system, in which case the leak was addressed until it could no longer be detected.

The time of each experiment was recorded with the start of the experiment defined by the initiation of the first heating ramp (Conditioning ramp). After 180 seconds, the second heating ramp (Heating ramp) was initiated. The igniter was turned on directly after the onset of the second heating ramp. Once self-sustained flaming ignition was visually confirmed, the igniter was left on for an additional 5 seconds after which it was immediately turned off. After a total test duration of 450 seconds, the pyrolyzer coil would be switched off and left to cool down back to ambient conditions. The particulate filter would then be removed and weighed to determine the mass of particulate residue that deposited on the filter. The combustor hood would subsequently be removed, allowing the removal of the ceramic crucible from the pyrolyzer coil system. The mass of the crucible would then be weighed, allowing the calculation of the char yield of the sample.



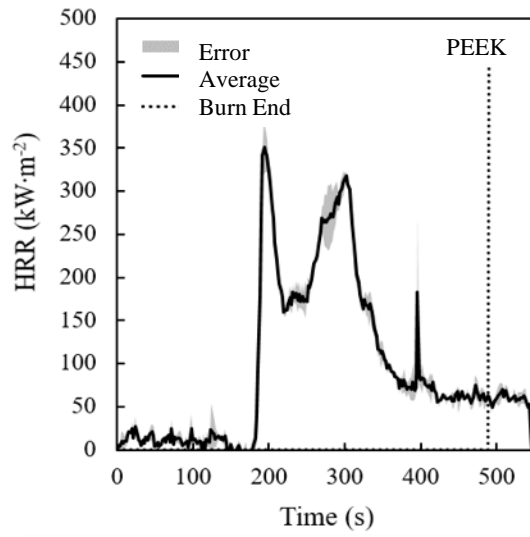
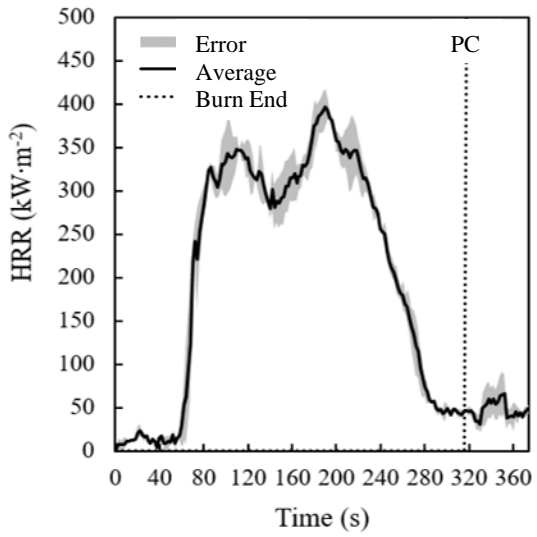
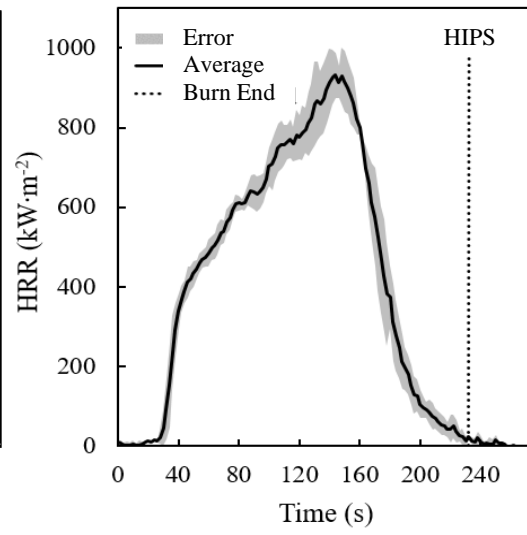
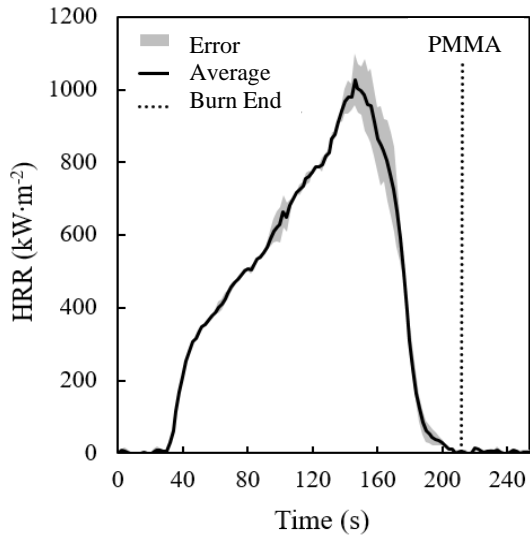
## 4 Chapter 4: Results and Analysis

### 4.1 Cone Calorimetry Results

HRR graphs were compiled using the raw HRR data obtained during each experiment, while the MLR graphs were constructed considering the time derivative of the sample mass. Both the HRR and MLR were normalized by the exposed sample area, i.e. 0.088 m<sup>2</sup>. The HRR and MLR graphs, along with the error, is presented per Figure 4.1 and Figure 4.2. The line labelled “Burn End” is the time that the experiment was visually confirmed to have ended. This time was defined as the point where decreased surface burning was noted. The standard error was calculated considered Equation (8).

$$Error = \frac{X_{max} - X_{min}}{2} \quad (8)$$

with  $X_{max}$  the maximum value and  $X_{min}$  the minimum value of a parameter. All uncertainty values in this report were roughly estimated using Equation 7 because, in the majority of cases, only two data points were collected for each quantity of interest.



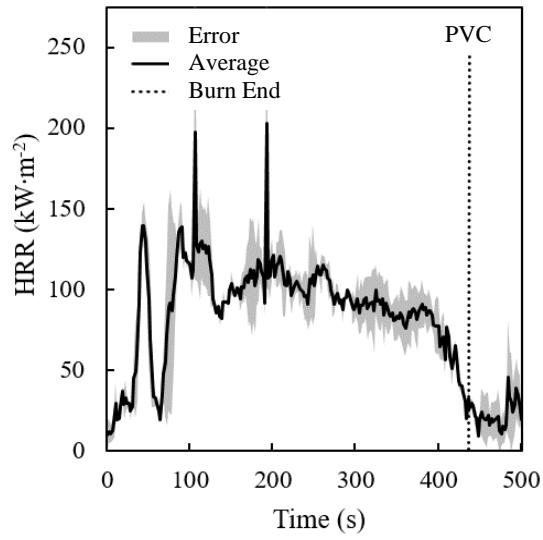
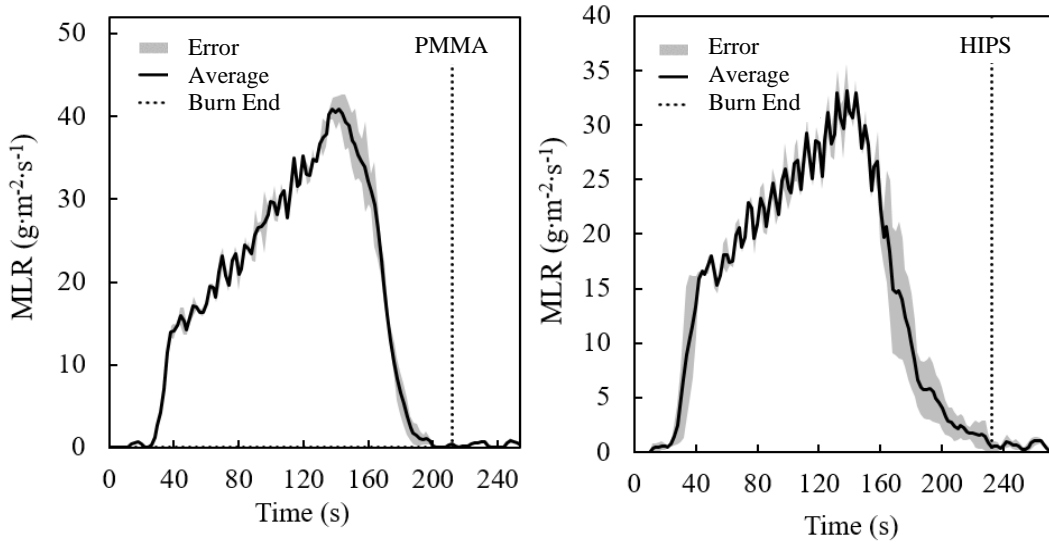


Figure 4.1: Cone calorimetry HRR profiles at an incident heat flux of  $50 \text{ kW}\cdot\text{m}^{-2}$ , using samples with thicknesses ranging from 2.8 – 3.05 mm



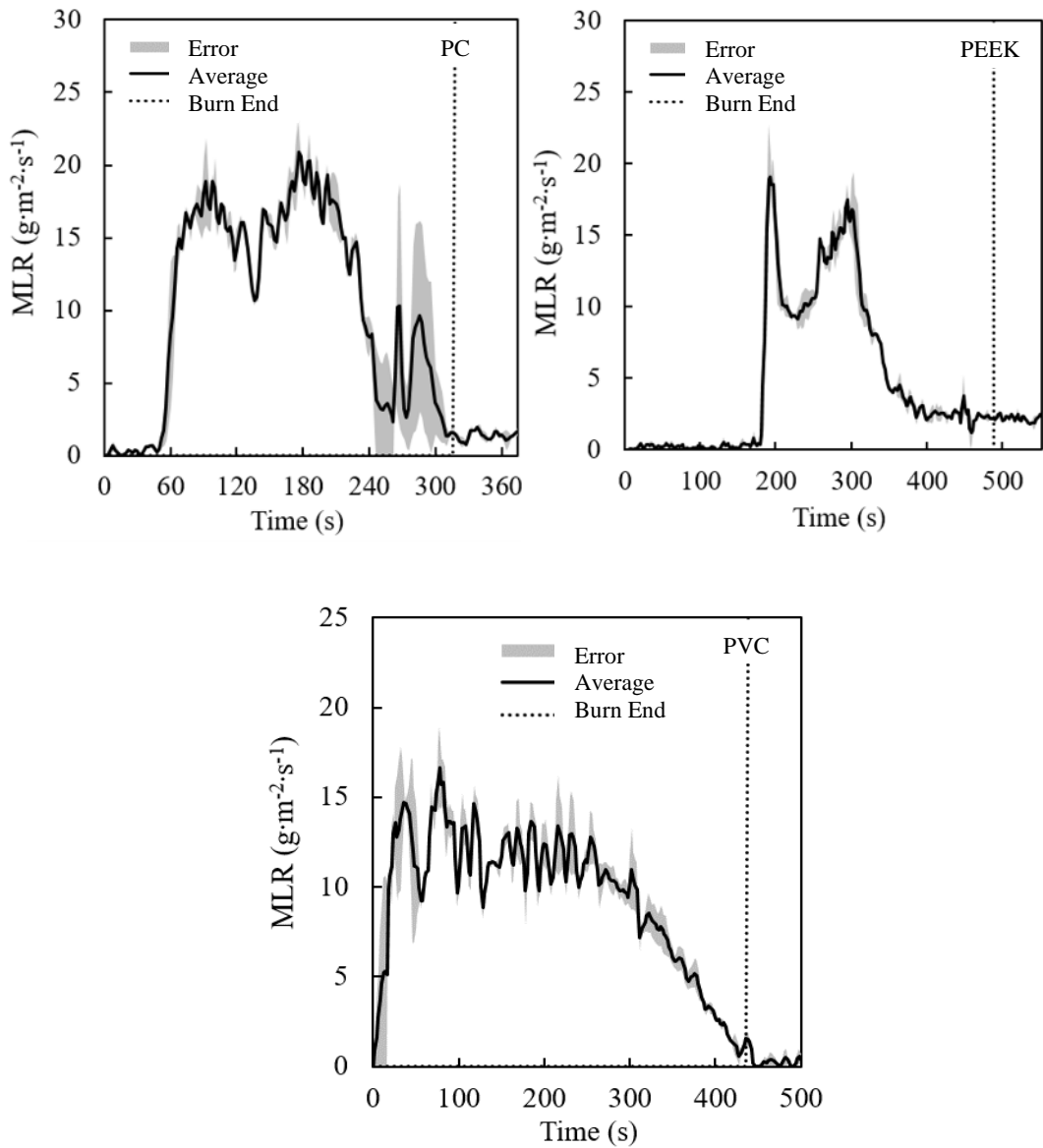


Figure 4.2: Cone calorimetry MLR profiles at an incident heat flux of  $50 \text{ kW}\cdot\text{m}^{-2}$ , using samples with thicknesses ranging from 2.8 – 3.05 mm

For each of the cone calorimeter experiments, the ignition time was recorded from visual observation. The HRR and MLR were then used to confirm the observed ignition times considering the initial rapid increases in both the HRR and MLR data. It

was noted that the recorded ignition time obtained from visual observation and the initial spikes in the HRR and MLR data were consistent. The recorded ignition times for each of the materials were averaged and are presented per Table 4.1, along with the calculated uncertainties.

The total smoke production for each of the cone calorimeter experiments was determined. It was calculated as the product of the smoke volume flowrate and the extinction coefficient. In turn, this quantity was integrated over a time range. The time range started at the recorded time to ignition up to the time indicated as “Burn End” for each material, as per Figure 4.3. The total smoke production was normalized by the initial mass of the sample. This final result is known as the average specific extinction area and is calculated using Equation (9) [23].

$$\sigma_{Average} = \frac{\int \dot{V}_i k_i dt}{m_{initial}} \quad (9)$$

with  $\sigma_{Average}$  the average extinction area ( $m^2 \cdot kg^{-1}$ ),  $\dot{V}_i$ , the instantaneous smoke volume flowrate ( $m^3 \cdot s^{-1}$ ),  $k_i$ , the instantaneous extinction coefficient ( $m^{-1}$ ) and  $m_{initial}$ , the initial mass of the sample (kg).

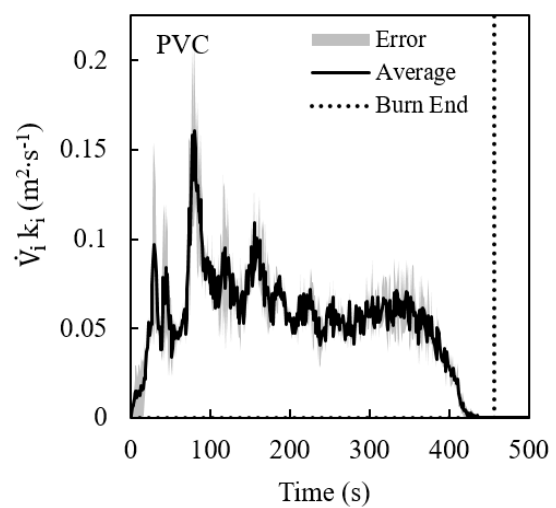
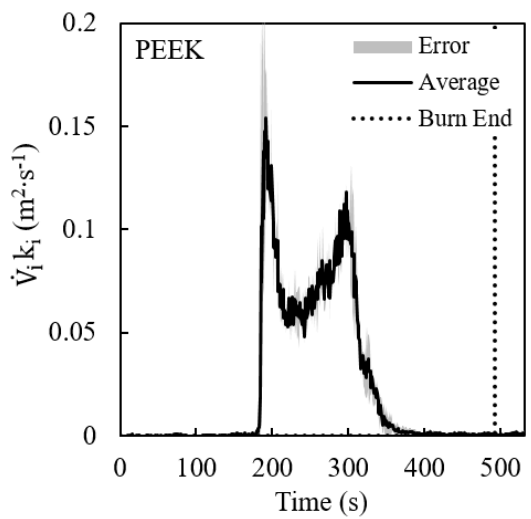
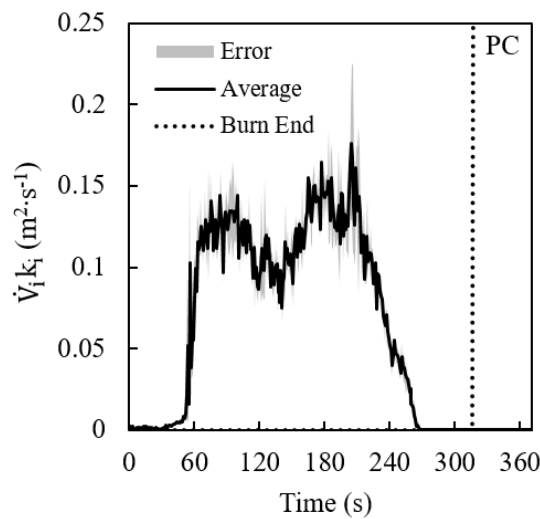
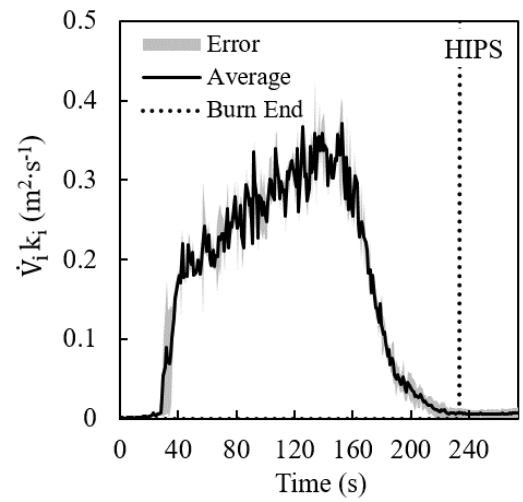
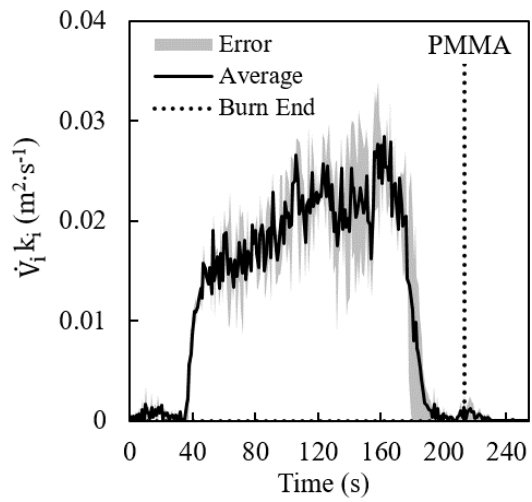


Figure 4.3: Cone calorimetry smoke production profiles at an incident heat flux of 50 kW·m<sup>-2</sup>, using samples with thicknesses ranging from 2.8 – 3.05 mm

The mass of char that formed during cone calorimeter tests was documented to provide the reader with a visual representation of the end product that was obtained for each material, as depicted per Figure 4.4. The final char yield was calculated by considering the MLR data and the initial sample mass. The final char yield was determined at the extinguishment time of each material indicated as “Burn End” on the MLR curves (see Figure 4.2). The char mass was calculated by subtracting the mass of the sample at this point from the initial sample mass. This char mass was normalized by the initial sample mass to provide the final char yield of each material.

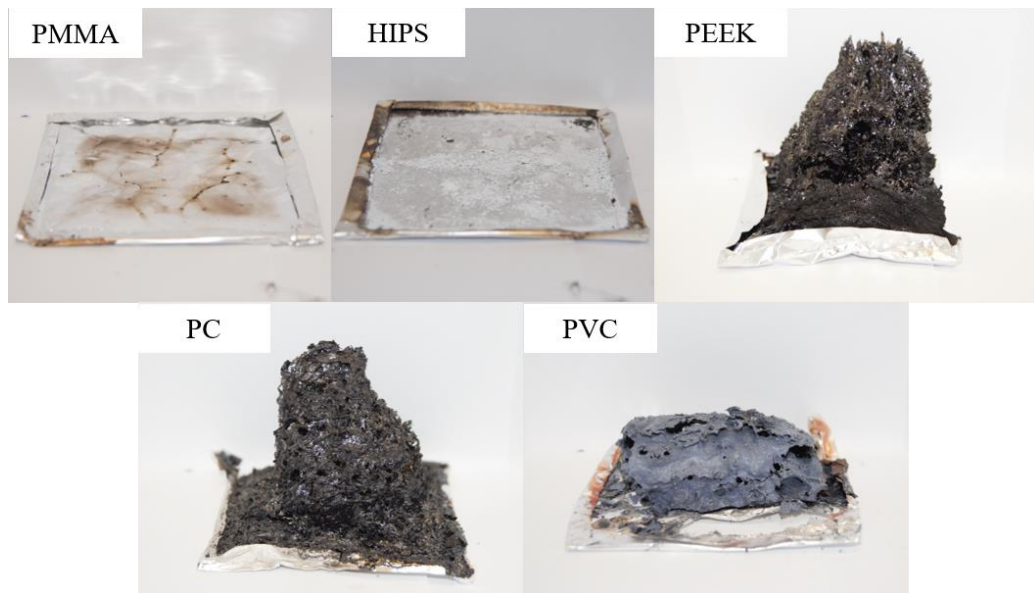
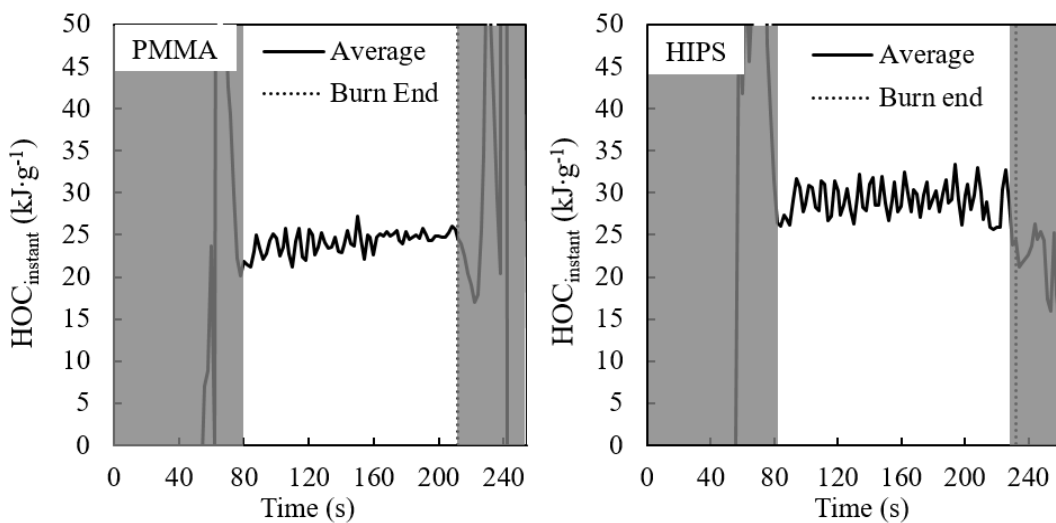


Figure 4.4: Photographs of final solid residue obtained in cone calorimeter experiments

The peak HRR was calculated as the maximum HRR value over a running average. The running average ranged over a period of 40 seconds which comprised 20 points. The average HRR was calculated over a running average, spanning from the time to ignition of the sample up to the extinguishment time indicated by the “Burn End” as presented in Table 4.1.

The instantaneous HOC ( $\text{HOC}_{\text{instant}}$ ) values for each of the cone calorimeter experiments was calculated through division of the instantaneous HRR by the corresponding instantaneous MLR data at each time interval. The HOC as normalized by the gasified mass for all of the cone calorimeter experiments was calculated by averaging a range of instantaneous HOC values over a time interval of steady burning as highlighted per Figure 4.5. The region of steady burning is indicative of complete surface burning i.e. the flames above the sample surface are spread across the entire sample surface. The HOC as normalized by the gasified mass values for each material is presented in Table 4.1





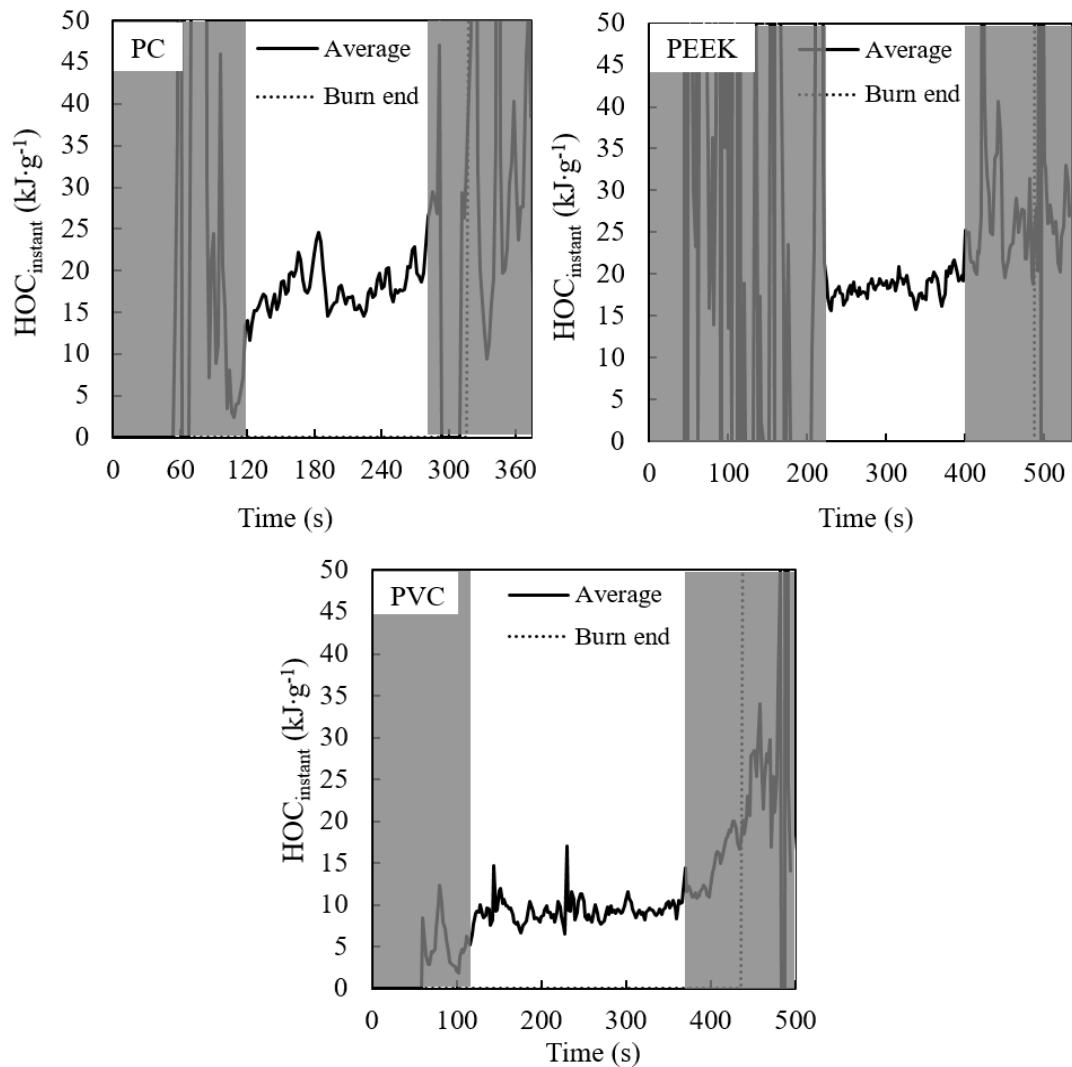


Figure 4.5: Cone calorimetry instantaneous HOC profiles at an incident heat flux of  $50 \text{ kW}\cdot\text{m}^{-2}$  used to calculate the HOC as normalized by the gasified mass

The HRR profiles (see Figure 4.1) were used to calculate the total heat release for each of the cone calorimeter experiments. The HRR profile was integrated over a time range spanning the recorded time of ignition up to the point indicated as “Burn End” for each material and subsequently multiplied by the exposed sample surface area

(0.088 m<sup>2</sup>). The HOC of a sample was calculated as the calculated total heat release for an experiment normalized by its corresponding initial sample mass.

Table 4.1: Cone calorimeter results of duplicate tests for all sample materials tested at 50 kW m<sup>-2</sup>

	PMMA	HIPS	PC	PEEK	PVC
Initial sample mass (g)	34.21 ± 0.33	31.03 ± 0.09	36.24 ± 0.20	41.81 ± 1.03	43.09 ± 0.14
Time of ignition (s)	29.5 ± 0.4	30.9 ± 3	68 ± 7	178.5 ± 3	35.5 ± 1
Burn End (s)	210 ± 13	234 ± 29	318 ± 6	495.3 ± 19	438 ± 12
Final char yield (%)	0.38 ± 0.09	1.69 ± 0.08	19.73 ± 0.22	52.88 ± 2.60	14.16 ± 0.51
Peak HRR (kW·m <sup>-2</sup> )	912 ± 51	844 ± 46	355 ± 14	269 ± 17	144 ± 8
Average HRR (kW·m <sup>-2</sup> )	515 ± 34	442 ± 28	210 ± 5	108 ± 0.4	86 ± 0.2
HOC (kJ·g <sup>-1</sup> initial mass)	24.16 ± 0.22	28.34 ± 1.1	15.90 ± 0.02	9.18 ± 0.22	7.89 ± 0.03
HOC (kJ·g <sup>-1</sup> gasified mass)	24.25 ± 0.24	29.14 ± 1.2	18.32 ± 0.04	18.50 ± 0.48	9.68 ± 0.20
$\sigma_{\text{Average}}$ (m <sup>2</sup> ·kg <sup>-1</sup> )	84 ± 15	1377 ± 151	782 ± 44	471 ± 21	676 ± 11

When considering the material flammability parameters presented in Table 4.1 for the five materials that are representative of a large range of polymeric materials the following is noted: the final char yield for the five materials ranges from near zero up to values exceeding 52% indicative of materials that were tested where the thermal

insulating effect of char could affect the HRR of a material. The peak HRR values for the five materials provide an indication as to the flammability of a material. It is noted that the peak HRR values range from 912 kW m<sup>-2</sup> for PMMA (most flammable) down to 144 kW m<sup>-2</sup> for PVC (least flammable). The  $\sigma_{Average}$  values reiterate that the five materials used represent a large set of polymeric materials as these values correspond to materials that burn with the production of small amounts of smoke (PMMA) as well as materials that are very sooty and produce large amounts of smoke (HIPS).

#### 4.2 Microscale Combustion Calorimetry Results

Raw HRR data was used to compile HRR graphs for each of the experiments and were processed to calculate the complete HOC normalized by the initial sample mass and the gasified mass. The HRR data was generated using the oxygen consumption principle. The onset HRR temperature was calculated at the first point where the HRR exceeded 5 W/g as depicted per Figure 4.6.

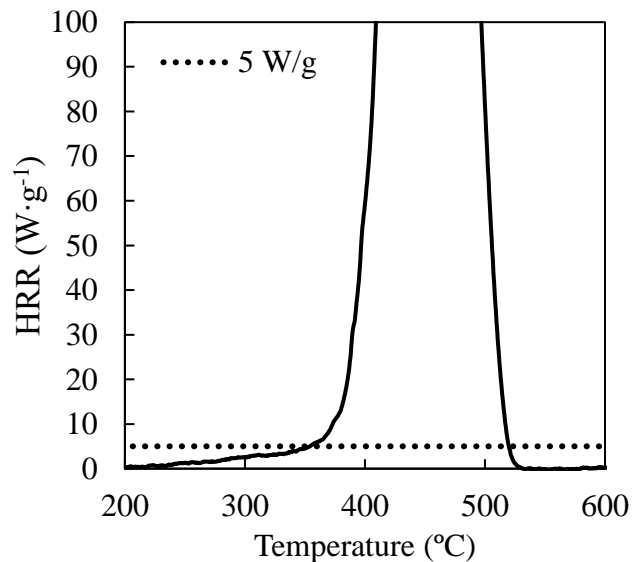
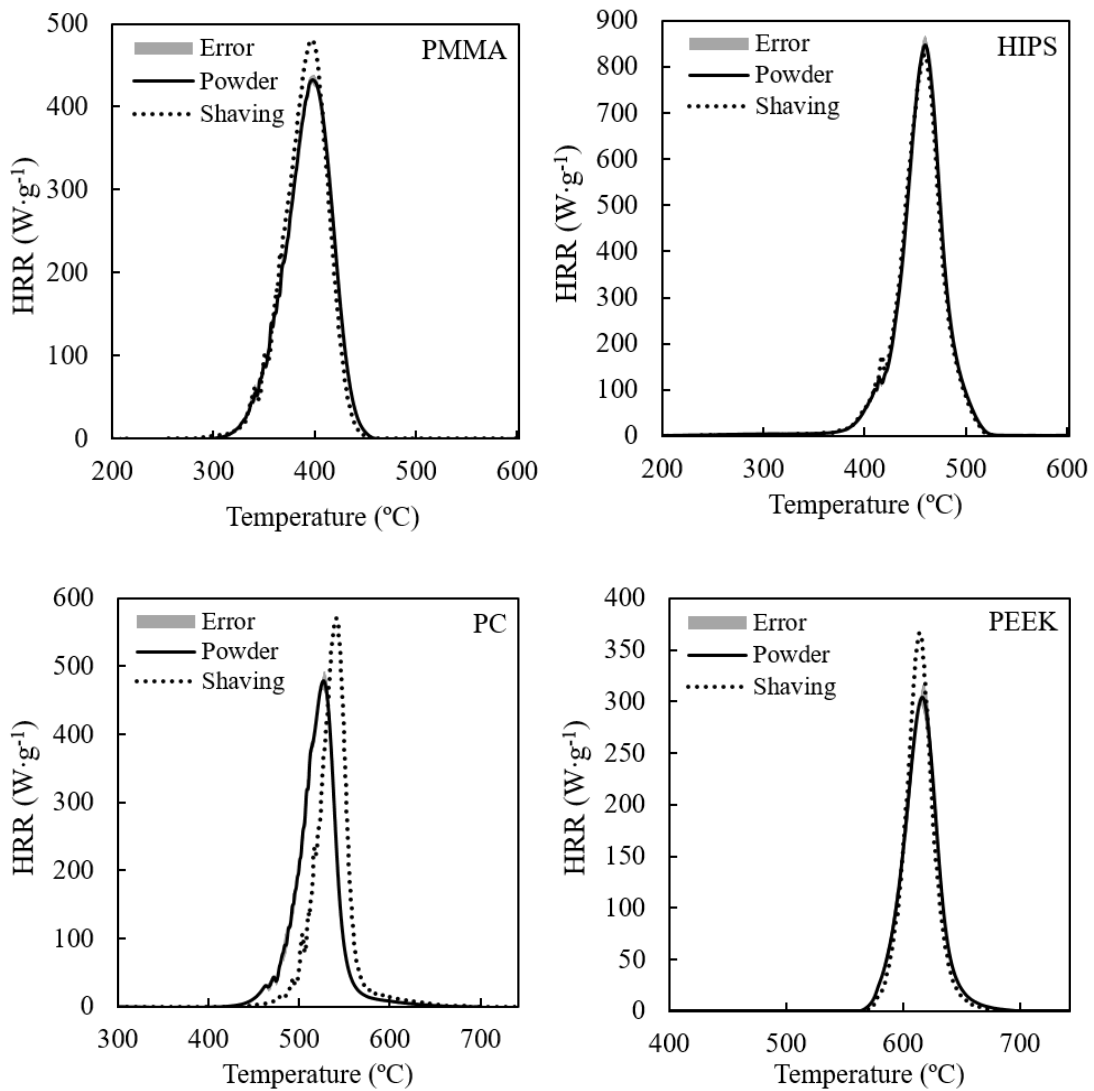


Figure 4.6: Criteria used to determine the onset HRR temperature for all the MCC tests which also indicates the limits of integration for each material

The HRR graphs for each of the materials for both the granulated powder samples and the sample shavings is presented per Figure 4.7. It should be noted that there is not a notable difference in the HRR profiles between the two sample geometries.



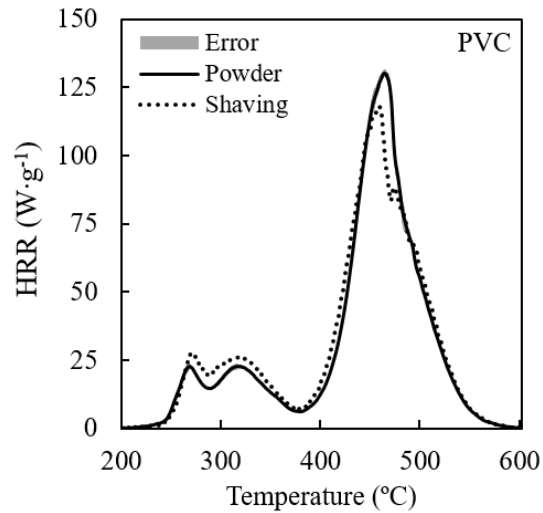


Figure 4.7: MCC HRR profiles for granulated powders and sample shavings for a heating rate of  $1\text{ °C}\cdot\text{s}^{-1}$  up to  $750\text{ °C}$  as normalized by the initial sample mass

The HRR data for both the granulated powder samples and the sample shavings were combined as there were no significant differences between the HRR profiles for both sample geometries. The error was calculated for the duplicate granulated powder samples with only a single experiment for each material being conducted using sample shavings. When considering Figure 4.7, it is noted that the peak HRR for each of the two sample geometries differ and will be analyzed independently. All material flammability data with the exception of the peak HRR for each of the two sample geometries will be combined into a single set of data. The peak HRR values for the granulated powder samples and the sample shavings will be separated by a slash as presented per Table 4.2. The first value corresponds to the granulated powder samples and the second that of the sample shavings.

The final char yield was calculated considering the mass of char at the end of each test. The end of all MCC experiments was reached when the maximum specified pyrolyzer temperature was reached i.e. 750 °C. The final char yield was calculated as the final char mass for each test being normalized by the initial sample mass.

The total heat released for each MCC test was calculated by integrating the HRR curve over a time range corresponding to a temperature range as depicted per Figure 4.7 after a baseline has been established between the first and last temperature range data point for each material. The same time range was used for all experiments considering a specific material. The normalized HOC for each sample was calculated by calculating the total heat released and normalizing it by the initial and gasified mass. The gasified mass was calculated as the difference between the initial sample mass and the calculated char mass for each sample

The average peak temperature and peak HRR were both calculated as the maximum HRR and maximum temperature value over a running average. The running average ranged over a period of 10 seconds which comprised 20 data points. The average HRR was calculated over the time range starting at the onset HRR temperature and ending at the last point after the peak HRR were the HRR is larger than  $5 \text{ W}\cdot\text{g}^{-1}$  as depicted per Figure 4.6.

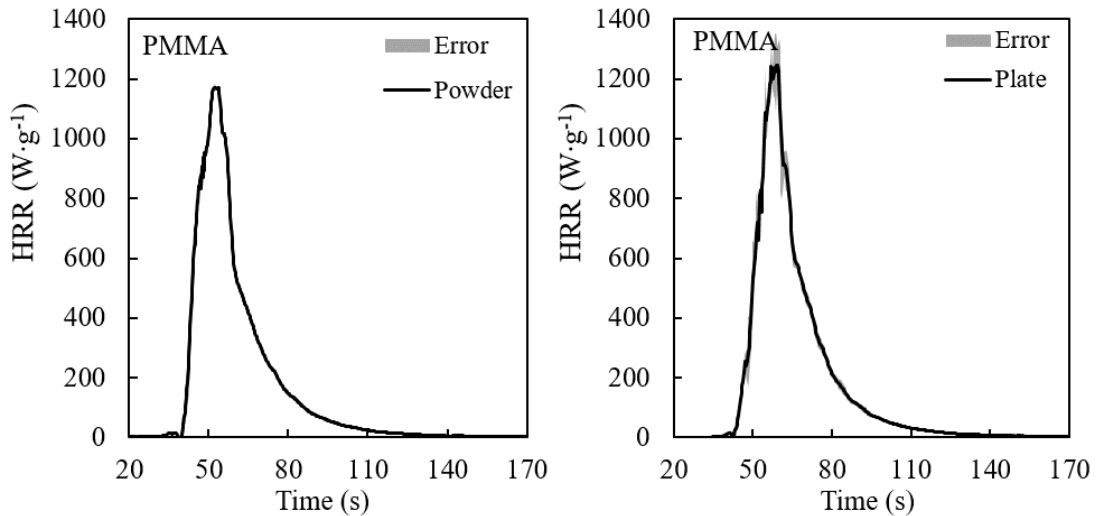
Table 4.2: MCC combined experimental results considering a heating rate of  $1\text{ }^{\circ}\text{C}\cdot\text{s}^{-1}$

	PMMA	HIPS	PC	PEEK	PVC
Initial sample mass (mg)	$3.89 \pm 0.15$	$3.76 \pm 0.02$	$4.67 \pm 0.33$	$4.64 \pm 0.42$	$4.80 \pm 0.3$
Final char yield (%)	$0.27 \pm 0.18$	$1.49 \pm 0.40$	$21.3 \pm 0.82$	$50.86 \pm 1.1$	$15.91 \pm 0.64$
Average peak temperature ( $^{\circ}\text{C}$ )	$398 \pm 0.5$	$458 \pm 0.3$	$534 \pm 8$	$616 \pm 2$	$462 \pm 3$
Peak HRR ( $\text{W}\cdot\text{g}^{-1}$ )	$431.4 \pm 6.0 / 472$	$841.5 \pm 19.8 / 821$	$476.1 \pm 12.9 / 565$	$305.0 \pm 9.2 / 361$	$130.3 \pm 1.5 / 118$
Onset HRR temperature ( $^{\circ}\text{C}$ )	$311 \pm 4$	$362 \pm 6$	$452 \pm 12$	$572 \pm 2$	$250 \pm 1.3$
Average HRR ( $\text{W}\cdot\text{g}^{-1}$ )	$175 \pm 2$	$238 \pm 4$	$119 \pm 0.4$	$111 \pm 6$	$37 \pm 0.7$
Complete HOC ( $\text{kJ}\cdot\text{g}^{-1}$ initial mass)	$24.45 \pm 0.40$	$39.3 \pm 0.45$	$21.2 \pm 0.47$	$10.13 \pm 0.09$	$11.42 \pm 0.23$
Complete HOC ( $\text{kJ}\cdot\text{g}^{-1}$ gasified mass)	$24.53 \pm 0.44$	$39.90 \pm 0.30$	$26.99 \pm 0.37$	$20.65 \pm 0.37$	$13.56 \pm 0.19$

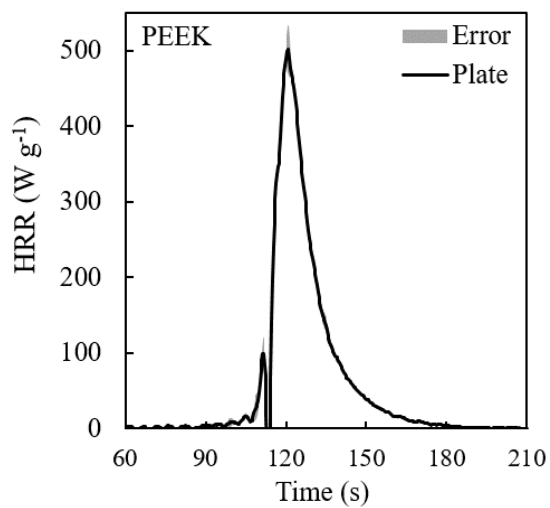
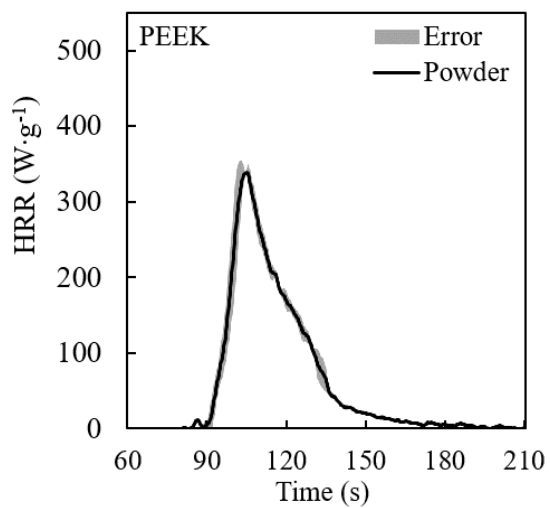
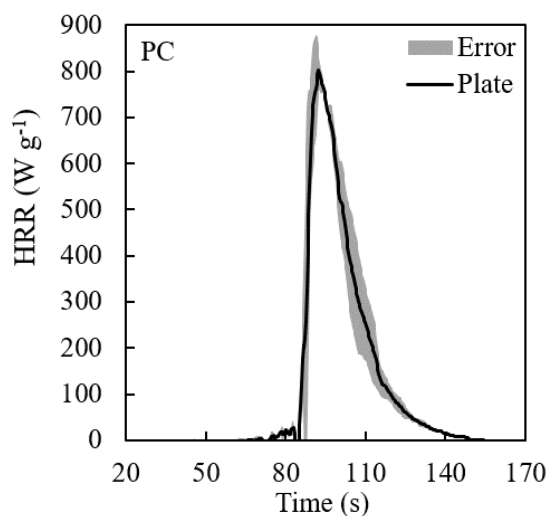
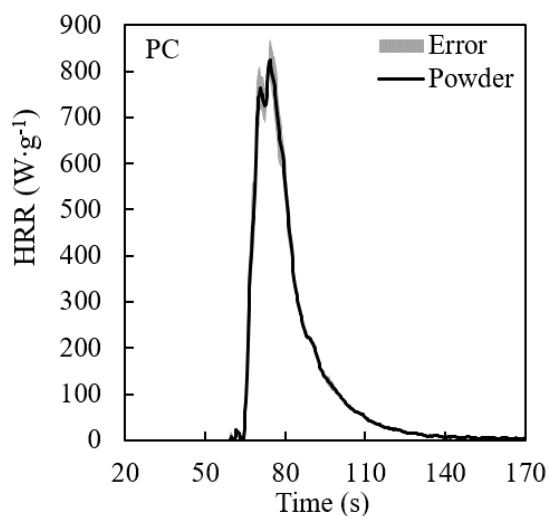
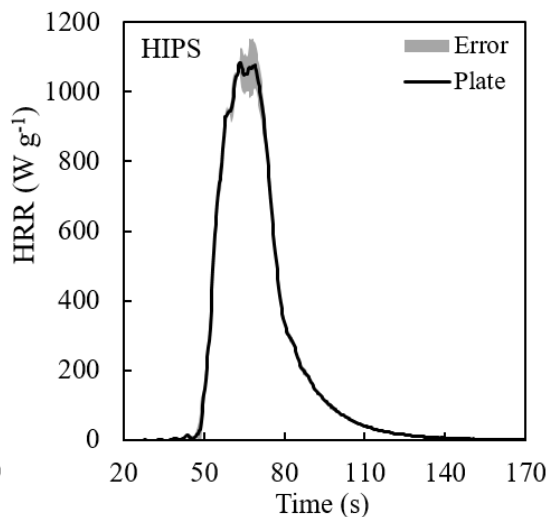
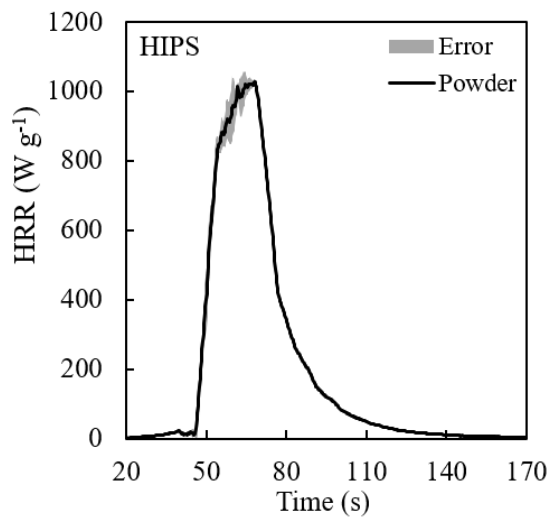
### 4.3 *Milligram-scale Flame Calorimetry Results*

The HRR was calculated using the oxygen consumption principle with both Method A and Method B originally being considered (see Section 1.2.4). The HRR graphs for both granulated powders and disk-like samples for each material is depicted per Figure 4.8.

The HRR graphs are plotted over the user-defined integration limits that were used during the calculation of the normalized HOC values for each sample. The integration limits were selected at 20 seconds and 170 seconds after the initiation of the second (Heating) ramp for all materials, with PEEK being the exception. The integration limits were selected considering the measured oxygen concentration before ignition of the sample and after extinguishment of the flame above the sample surface. The instantaneous change in the oxygen concentration at both these points was near zero. The integration limits used for PEEK were 60 seconds and 210 seconds after initiation of the second (Heating) ramp. They were selected knowing that PEEK is the material within the material test matrix that decomposes at the highest temperature, and this requires the integration limits to shift towards a higher time range. The time axis starts at the time after the initiation of the second heating ramp (that is, this time axis does not include the time of the Conditioning ramp).







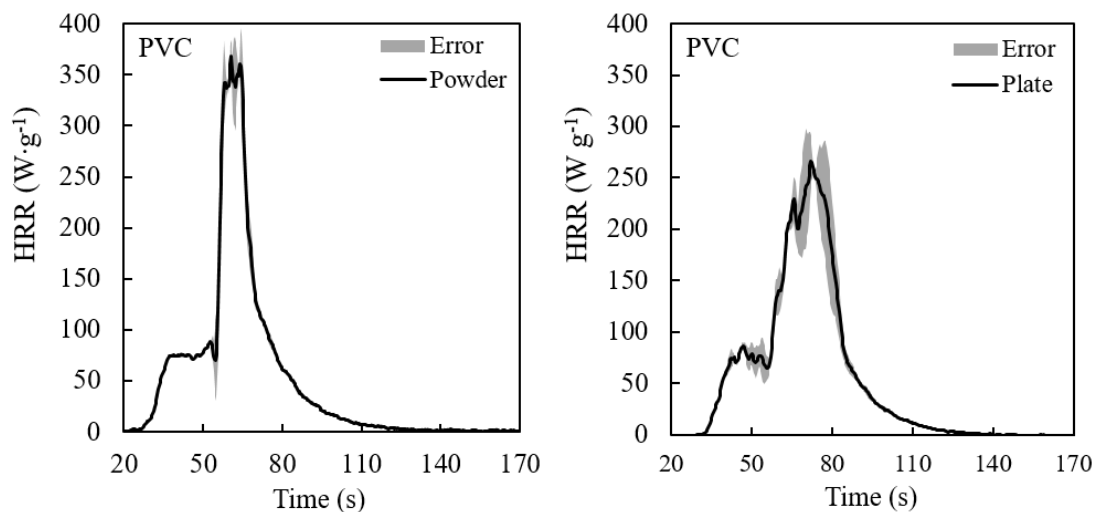
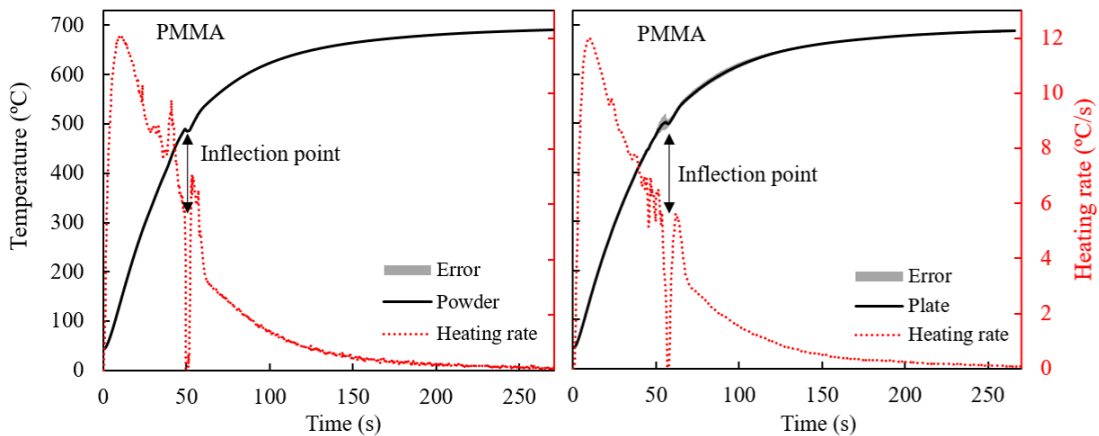
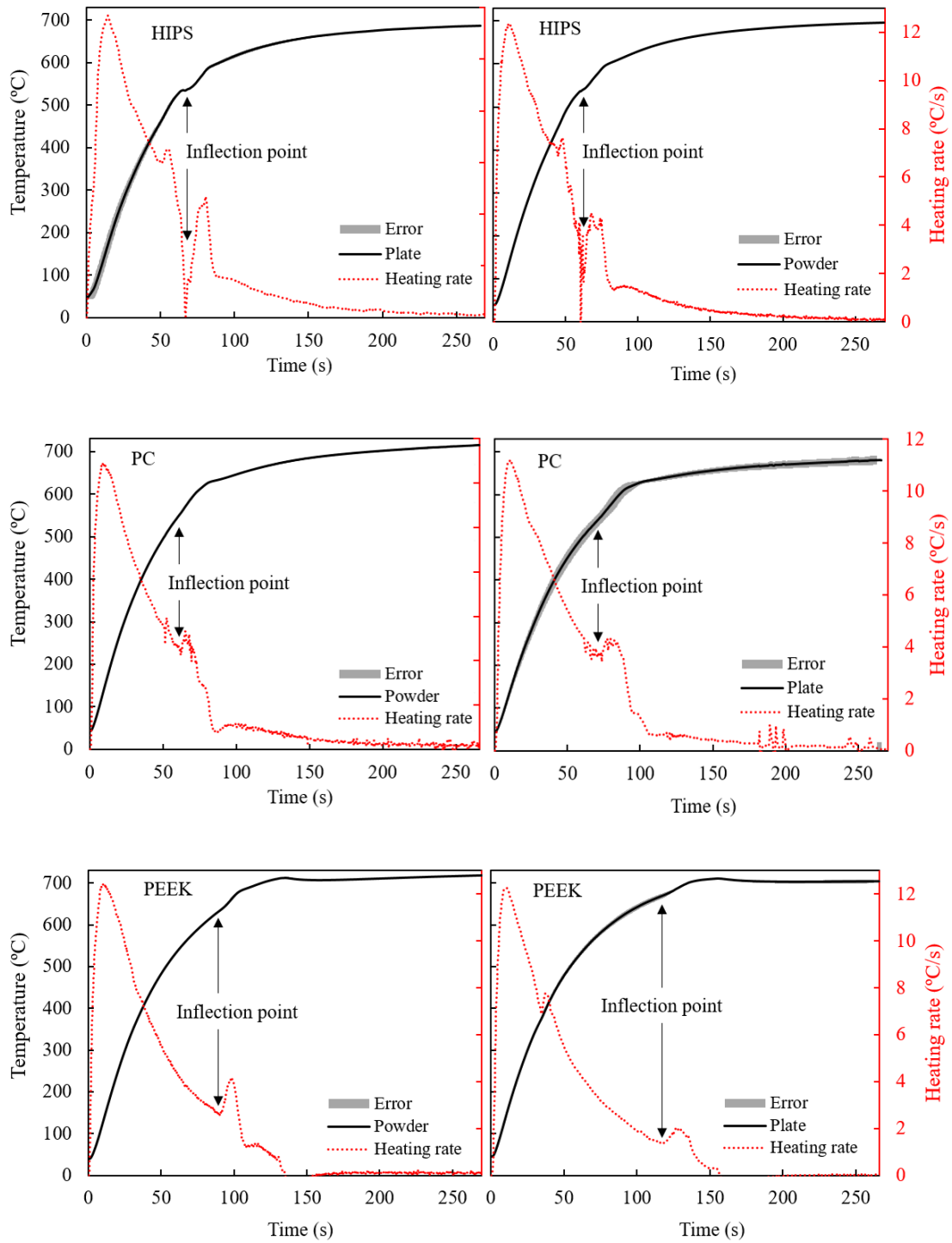


Figure 4.8: MFC HRR profiles as normalized by the initial sample mass for granulated powder- (left) and disk-like plate (right) samples for each material obtained using Method B after the initiation of the Heating ramp

The time interval for each of the graphs corresponds to the integration limits over which the normalized HOC for each of the sample was calculated. The normalized HOC values for each sample was calculated by numerical integration of the corresponding HRR profile and dividing it by either the initial sample mass or the gasified mass. The normalized HOC for each sample was calculated considering both Method A and Method B. It was noted that both Method A and B provided essentially identical normalized HOC values. It was however noted that the HRR profiles obtained using Method A exhibited a negative HRR at the onset of combustion of the sample. This negative HRR is attributed to the gas displacement of air in the chamber [17]. The HRR profiles for Method B, as depicted per Figure 4.8, are free of this phenomenon and were considered for all further calculations.

The measured surface temperature profiles, as well as the corresponding heating rate profiles, are presented per Figure 4.9. The granulated powder sample temperatures, as well as the disk-like plate temperatures, were initially analyzed separately. When visually comparing the peak HRR profiles for both geometries of each material, it is noted that the peak HRR for both geometries of PMMA, HIPS and PC are fairly similar. This is not the case for PEEK and PVC. The peak HRR for the disk-like PEEK plates is larger than for the granulated powder samples. This could potentially be attributed to the delayed release of combustible gases as a result of the thermal insulating effect of the intumescent char being more prominent for the disk-like plate sample than that for the granulated powders. This delayed release is apparent when considering the time at which the HRR rapidly increases for both sample geometries. A smaller peak HRR for disk-like PVC plates when compared to the peak HRR of the granulated powder sample geometry could also be attributed to the insulation effect of the char being more prominent for the disk-like plates.





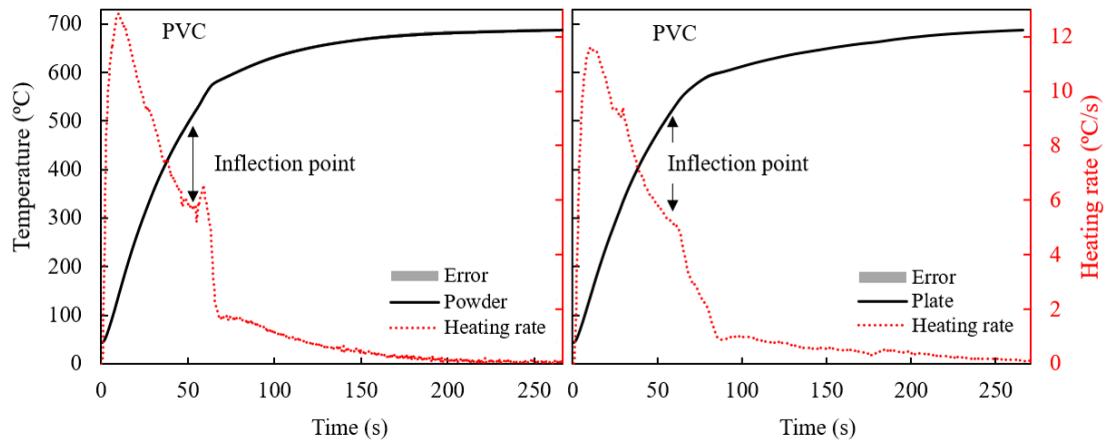


Figure 4.9: Measured surface temperature profiles and the corresponding heating rate profiles for both sample geometries of each material in the MFC

The inflection point on the temperature graph corresponded to an abrupt decrease in the heating rate as highlighted in Figure 4.9. The heating rate for each corresponding temperature profile was considered as this emphasized the inflection point region better than the actual temperature profile. The inflection point corresponds to the peak HRR temperature region. It was later concluded that the peak HRR temperature for both sample geometries was sufficiently similar and was combined as a single set of temperatures presented in Table 4.3. It was further noted that the time at which the abrupt decrease in the heating rate occurred for the disk-like plates corresponded more accurately with the calculated average peak HRR temperature than that for the granulated powder samples

The char yield was calculated by normalizing the mass of the sample at the end of the experiment by the initial sample mass. The particulate yield was calculated by the normalization of the total particulate mass deposited on the filter by the initial mass

of the sample. The average peak HRR as well as the average peak HRR temperature was calculated as the maximum HRR and maximum temperature over a running average. The running average spanned over a period of 7 seconds, which comprised 20 data points. The average HRR was calculated over the time range starting at the identified time to ignition for each sample and ending at the upper integration limit used to calculate the corresponding normalized HOC.

The measured ignition temperature of a sample was obtained by calculating the time to ignition of a sample considering the percentage of O<sub>2</sub> consumed during a test. A sample was said to have ignited once the difference between the baseline O<sub>2</sub> concentration, calculated prior to the initiation of the second heating ramp, and the instantaneous O<sub>2</sub> concentration percentage was greater than 0.1%.

Data was obtained for the samples run in duplicates for both the granulated powder samples and the disk-like plates. All material flammability parameters, with the exception of the peak HRR and time to ignition data, were combined into one data set and is presented per Table 4.3. The parameters that will be analyzed independently have been separated by a slash with the first value being for the granulated powder samples and the second for the disk-like plates.

Table 4.3: MFC experimental results for both sample geometries considering a maximum heat flux of  $50 \text{ kW}\cdot\text{m}^{-2}$

	PMMA	HIPS	PC	PEEK	PVC
Initial sample mass (mg)	$34.51 \pm 0.66$ $/40.04 \pm 0.47$	$35.31 \pm 0.5$ $/38.89 \pm 0.71$	$35.57 \pm 0.62$ $/33.78 \pm 4.1$	$35.35 \pm 0.55$ $/55.38 \pm 3.5$	$35.9 \pm 0.62$ $/57.08 \pm 5.8$
Time to ignition (s)	$43.8 \pm 1.1$ $44.0 \pm 1.1$	$49.2 \pm 0.8$ $49.0 \pm 0.8$	$66 \pm 0.2$ $86.0 \pm 0.3$	$93 \pm 0.6$ $115.0 \pm 0.6$	$37.8 \pm 0.5$ $/38.0 \pm 0.5$
Char yield (%)	$0.33 \pm 0.09$	$4.99 \pm 1.21$	$17.27 \pm 3.54$	$49.91 \pm 2.85$	$17.27 \pm 2.12$
Particulate yield (%)	$1.12 \pm 0.46$	$12.23 \pm 2.41$	$7.48 \pm 0.64$	$1.81 \pm 1.37$	$4.06 \pm 2.18$
Ignition temperature ( $^{\circ}\text{C}$ )	$439 \pm 11$	$473 \pm 8$	$576 \pm 6$	$652 \pm 11$	$392 \pm 8$
Peak HRR ( $\text{W}\cdot\text{g}^{-1}$ )	$1123 \pm 6$ / $1155 \pm 30$	$1018 \pm 24$ / $1073 \pm 51$	$752 \pm 26$ / $764 \pm 50$	$336 \pm 6$ / $448 \pm 13$	$328 \pm 18$ / $269 \pm 2$
Peak HRR temperature ( $^{\circ}\text{C}$ )	$497 \pm 7$	$544 \pm 11$	$603 \pm 0.5$	$678 \pm 4$	$582 \pm 2$
Average HRR ( $\text{W}\cdot\text{g}^{-1}$ )	$507 \pm 5$	$553 \pm 20$	$428 \pm 19$	$249 \pm 43$	$221 \pm 20$
HOC ( $\text{kJ}\cdot\text{g}^{-1}$ initial mass)	$24.18 \pm 0.70$	$29.39 \pm 1.56$	$15.15 \pm 0.5$	$8.49 \pm 0.23$	$7.42 \pm 0.48$
HOC ( $\text{kJ}\cdot\text{g}^{-1}$ , gasified mass)	$24.27 \pm 0.68$	$30.27 \pm 1.25$	$18.56 \pm 0.59$	$17.57 \pm 0.53$	$9.27 \pm 0.21$

When considering the material flammability parameters obtained with the use of the MFC and summarized in Table 4.3, it is again noted that the five materials used during this study is representative of a large range of polymeric materials. It was noted that the calculated time to ignition and peak HRR values were significantly different for both sample geometries and were analyzed independently. It is noted that when the time to ignition for disk-like plates is larger than that for the granulated powders, the peak HRR for the disk-like plates is also larger than that of the granulated powders (PC and PEEK). This could be attributed to the insulating effect of the intumescent char which suggests that this physical effect is captured in using the MFC test technique. The peak HRR values for the MFC follow the same trend as that noted for the peak HRR values of the cone calorimeter test. The peak HRR is indicative of the flammability of a material with PMMA being the most flammable and PVC the least flammable of the five materials tested.

## 5 Chapter 5: Comparative analysis of Cone calorimetry, MCC and MFC data

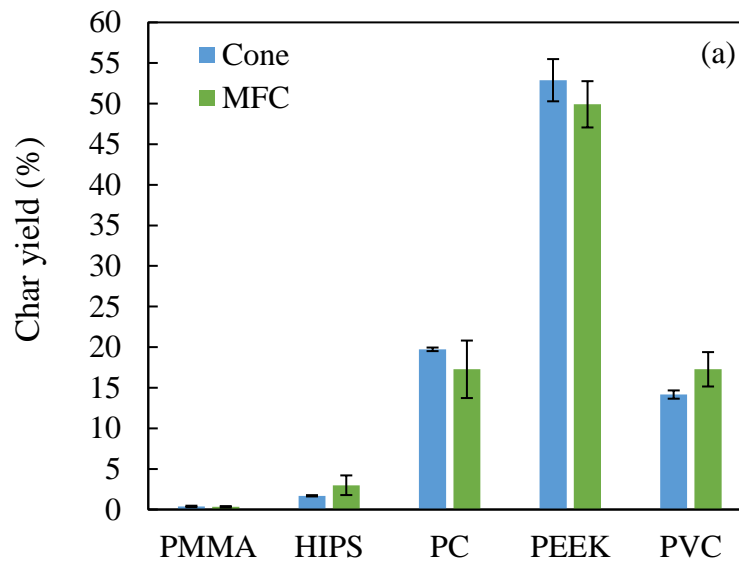
The present study seeks to improve the limited use of the MFC with the introduction of a newly designed flat radial pyrolyzer coil. The new pyrolyzer coil was envisioned to more closely approximate the burning behavior of a material sample in the cone calorimeter. The comparative analysis of the data processed from the cone calorimeter, MCC, and MFC experiments had one main objective: to quantitatively



verify whether the modified MFC captures the burning behavior of a sample in the cone calorimeter.

### 5.1 *Char yields*

The char yield is an intensive property of a material, and it is therefore expected that the calculated char yield for each material in the MFC, MCC and cone calorimeter should be approximately equal. The char yield is a material property that can also be used to verify whether all the volatiles have been released from the pyrolyzing material, thereby providing an indication as to the efficiency of the combustion process. The char yield of each material from the cone calorimeter tests has been compared to the yields obtained in both the MFC and MCC, as per Figure 5.1.



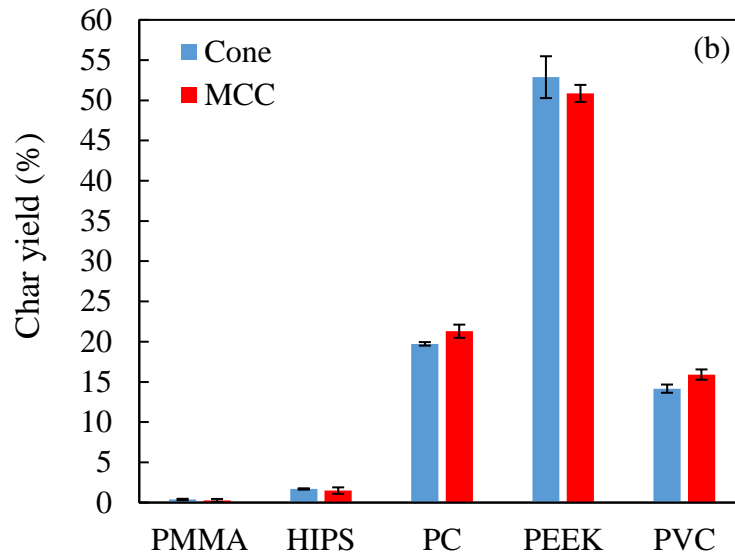


Figure 5.1: Char yields for the (a) MFC and (b) MCC compared to the yields obtained in the cone calorimeter

From Figure 5.1, it is noted that, from the comparison of the cone calorimeter and MCC, the char yields are in slightly better agreement than the comparison considering the MFC. The larger variation in the MFC char yields for PC and PVC can be attributed to the potential oxidative pyrolysis of the intumescent char before the onset of flaming ignition of the sample for the case of PC. It was noted that the char swelled, rising above the lip of the quartz tube housing. The presence of the hot wire igniter above the lip of the quartz tube could have potentially accelerated this process until flaming combustion became the dominate process.

## 5.2 *Normalized heats of combustion*

The HOC is another intensive property of a material and can be directly compared across different material testing techniques. The HOC of a material is typically used to

determine the combustion efficiency of a material. The calculated HOC values normalized by the initial sample mass for each material from the cone calorimeter is compared to the values obtained using MFC and MCC, as per Figure 5.2. The analysis of the HOC values will provide insight as to the how well the modified MFC captures the gas- and condensed phase burning behavior of materials being considered in comparison to cone calorimeter tests.

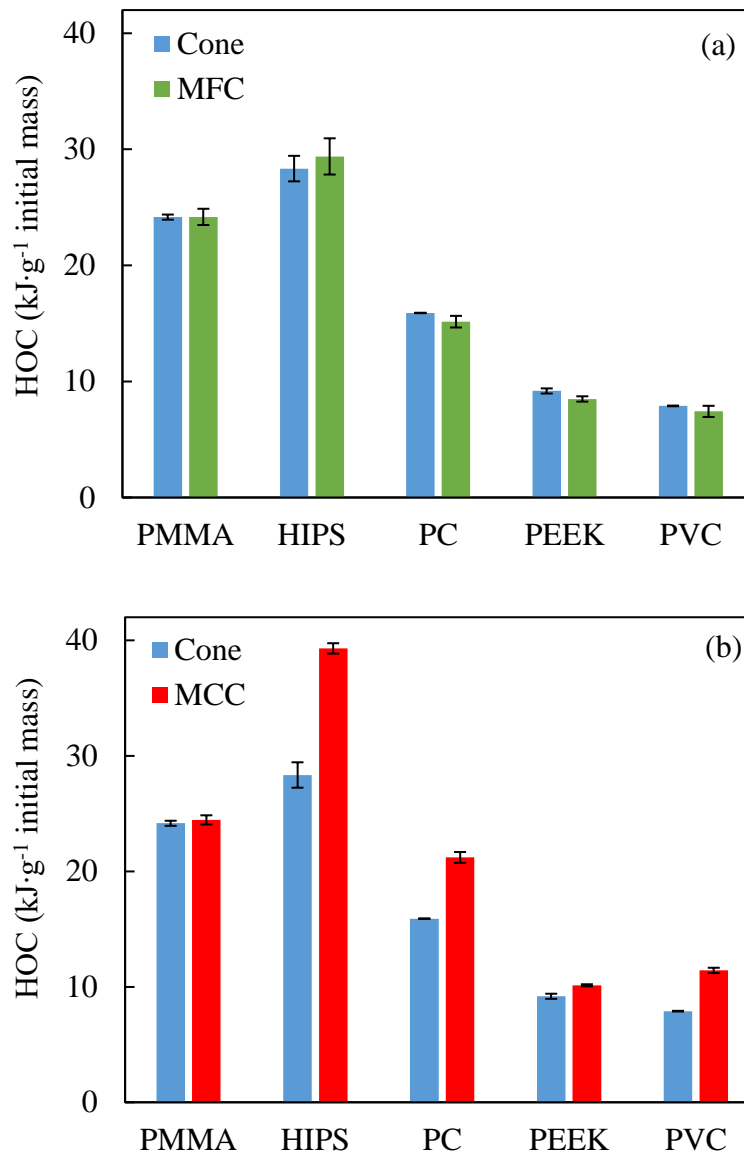
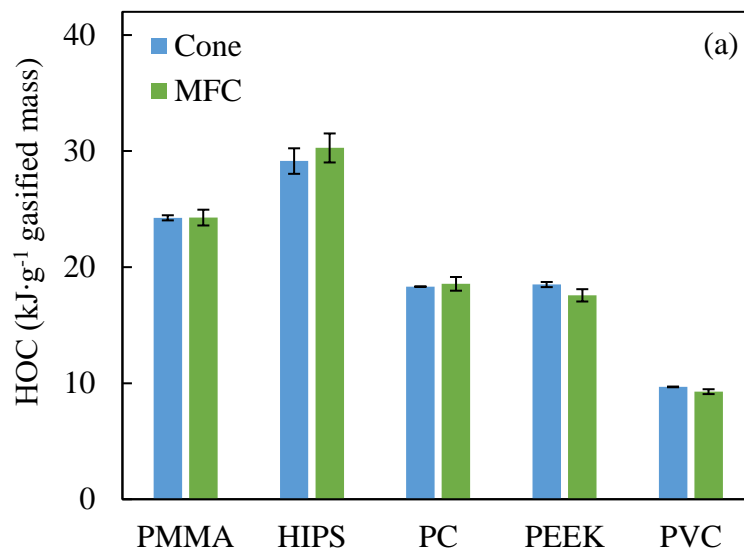


Figure 5.2: HOC data for (a) MFC and (b) MCC experiments as normalized by the initial sample mass and compared to the values obtained in the cone calorimeter

As noted in Figure 5.2, the MFC more closely approximates the HOC values of the materials when tested in the cone calorimeter. This is not the case when the MCC HOC values are compared the HOC values of the cone calorimeter. The MCC is used to obtain values for the normalized HOC of a material by driving the combustion process to completion. The MCC therefore does not sufficiently capture the incomplete combustion process associated with the flaming combustion process of a sample. The MFC is a test that allows for the study of the flaming combustion of a material. It is therefore expected that the normalized HOC values calculated from the MFC experiments will more accurately capture the incomplete flaming combustion process of a material as noted in the cone calorimeter. The HOC values normalized by the total gasified mass of a sample from the MFC and the MCC were directly compared to the HOC values obtained in the cone calorimeter, as depicted per Figure 5.3.



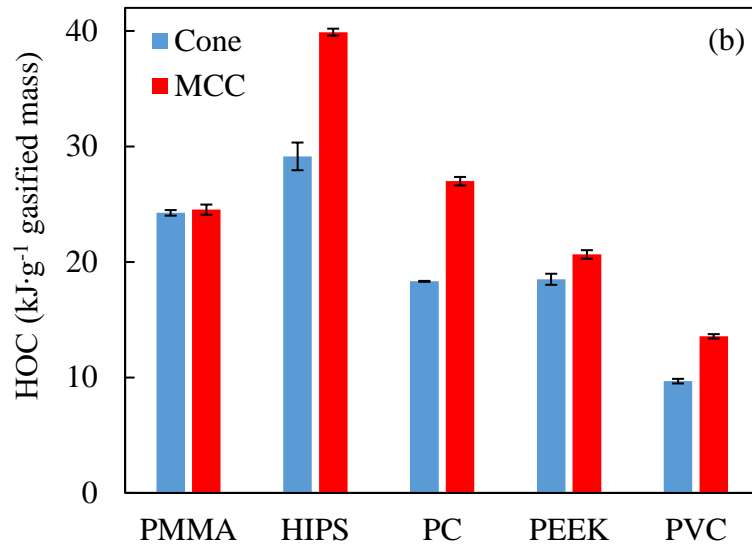


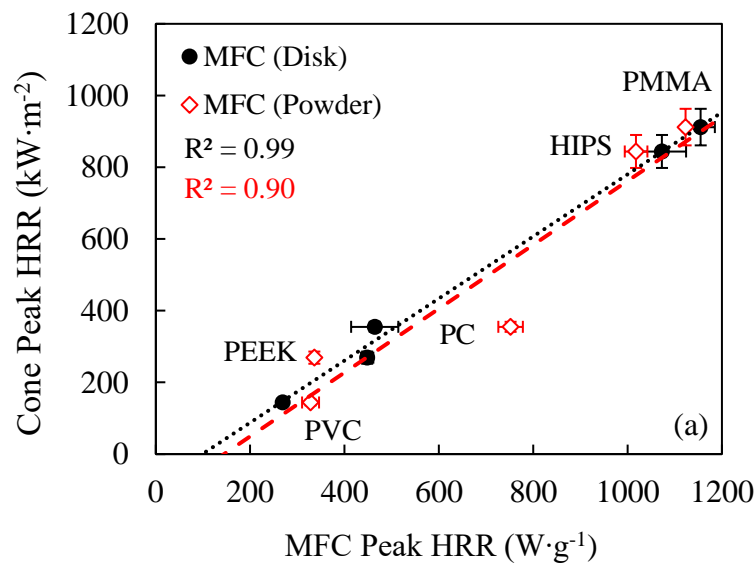
Figure 5.3: HOC data for (a) MFC and (b) MCC experiments as normalized by gasified mass of the sample and compared to the values obtained in the cone calorimeter

It is again noted that the calculated normalized HOC values from the MFC are very similar to the values from the cone calorimeter when compared to the HOC values calculated from the MCC. This is expected as the gasified mass for each sample is calculated considering the corresponding char yield. As the MFC and MCC experiments both capture similar char yields to that of the cone calorimeter experiments, the HOC normalized by the gasified mass is expected to be proportionally larger than the HOC values normalized by the initial sample mass for any material producing char.

### 5.3 Peak and average HRR

The peak HRR is another important parameter used to quantify the maximum rate at which heat energy is being released during the combustion process of a material.

It provides a measure of the intensity of the combustion process. The peak HRR for the granulated powders and the sample shavings (MCC) or the disk-like plates (MFC) was analyzed separately as variations between sample geometries was noted. The comparison of peak HRR of a material in cone calorimeter tests with materials tested in the MFC and MCC is depicted per Figure 5.4, for both sample geometries. A linear trend was expected between the peak HRR values obtained from the cone calorimetry experiments and the peak HRR values from the MFC experiments. A linear fit between the peak HRR values from the cone calorimeter and the values from the MCC was performed to quantitatively compare the linear correlations between the MFC and MCC data as presented per Figure 5.4.



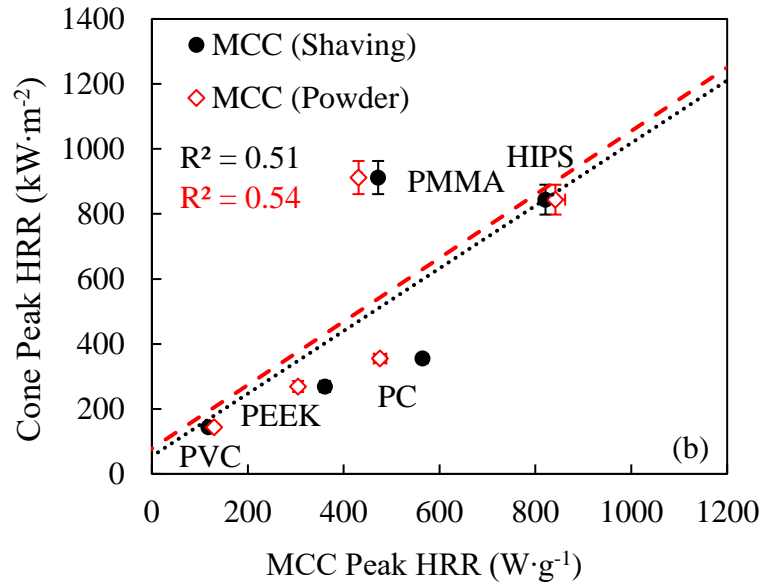


Figure 5.4: Peak HRR values from the cone calorimeter compared with peak HRR values for (a) MFC, (b) MCC

It is noted that the coefficient of determination,  $R^2$ , of the comparison between MFC and cone calorimeter results is much higher than the comparison considering the MCC, which indicates that the MFC better predicts the peak HRR results expected from cone calorimeter tests. This was true for both the granulated powder samples and the disk-like plates. This could be attributed to the incomplete gas-phase combustion as well as the impact of the char formation on the transport of heat and gaseous decomposition products being more accurately captured in the MFC as well as the heating rate of the MFC being in closer agreement to cone calorimetry experiments than that of the MCC. It was further noted that the correlation between the cone calorimeter tests and the MFC using disk like plates was better ( $R^2 = 0.99$ ) than the correlation considering the MFC granulated powder samples ( $R^2 = 0.9$ ). This

observation can be explained considering the peak HRR for the two sample geometries compared to their documented time to ignition as depicted per Figure 5.5. It is noted that for PC, PEEK and PVC, both charring materials, the time to ignition values for the disk like plates are higher than that for the granulated powders. The increased time to ignition values corresponded to an increased peak HRR. This could be as a result of the disk-like plates more accurately capturing the insulation effect of the char formation on the transport of gaseous decomposition products through the char – the formation of char delays the release of combustible gases. At the time corresponding to time to ignition of a material, the rate at which the combustible gases are being produced are larger for the disk-like plates than for the powders as indicated by a higher peak HRR.

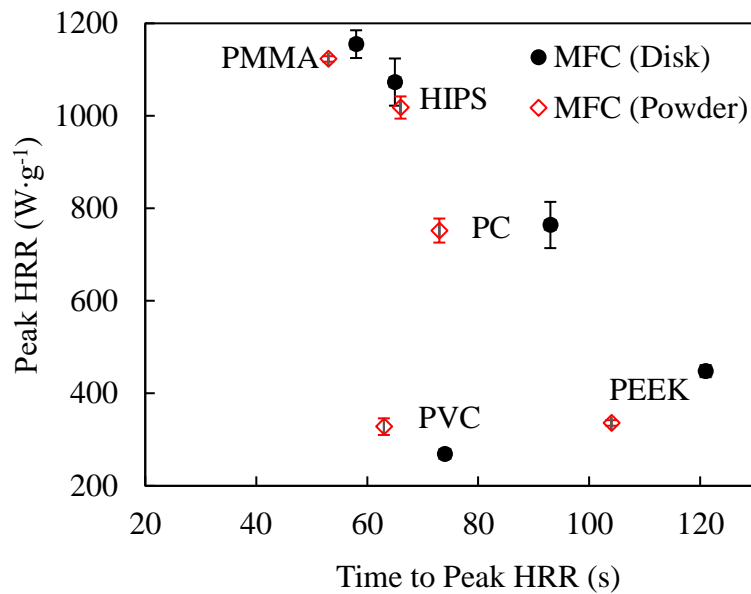


Figure 5.5: Peak HRR as a function of the time to ignition for both MFC sample geometries



The average HRR for each of the sample geometries in both the MFC and MCC was analyzed. It was, however, noted that average HRR values obtained in the cone calorimeter compared to either the MFC or MCC values did not correlate with one another. For this reason, the average HRR data will not be considered for further analysis.

#### 5.4 Ignition temperature and time-to-ignition

The ignition temperature and time-to-ignition for a material is an extensive property of a material that is expected to change with sample size i.e. the sample mass and the defined heating rate of the sample. A correlation between the cone calorimeter time to ignition data and the ignition temperature for the MFC experiments or the onset HRR temperature for the MCC experiments was considered. One explicit way to correlate these two parameters is with the use of the ignition theory as presented in Equation (10). When considering the use of the analytical ignition theory, the sample must be assumed to be either thermally thin or thermally thick. Cone calorimetry experiments make use of samples that are considered thermally thick. Considering this, it was assumed that the samples used during MCC and MFC experiments were more representative of thermally thick samples allowing for direct comparison between the different flammability tests. The ignition temperature for the MFC data and the onset HRR temperature data for the MCC were both labelled as  $T_{ig}$  (°C) for purpose of calculation. The ambient temperature ( $T_o$ ) was assumed to be equal to 25 °C. The time to ignition data for the cone calorimeter experiments was labelled as  $t_{ig}$  (s) for these calculations.

$$t_{ig} = \frac{(\pi/4)(k\rho c)(T_{ig} - T_o)^2}{\dot{q}''^2} \quad (10)$$

If one assumes the thermal inertia ( $k\rho c$ ) of each material to be constant as well as the incident heat flux ( $\dot{q}''$ ) for cone calorimetry, MFC and MCC, then Equation (10) suggests a linear relationship between the time to ignition and the square of the temperature difference ( $T_{ig}-T_o$ ). Since ignition temperature for cone calorimetry experiments could not be measured due to challenges associated with such a measurement, the ignition time measured in cone calorimetry tests is compared to the square of the temperature difference ( $T_{ig}-T_o$ ) measured from MCC and MFC. By performing this comparison, one can identify if either MCC or MFC can approximate the thermally thick ignition behavior, as well as which of these techniques is better aligned with the burning behavior of samples in cone calorimetry experiments. The MFC ignition temperatures as well as the MCC onset HRR temperatures were compared to the cone calorimeter times to ignition data for all materials. Least square fitting was performed with a linear function as depicted per Figure 5.6.

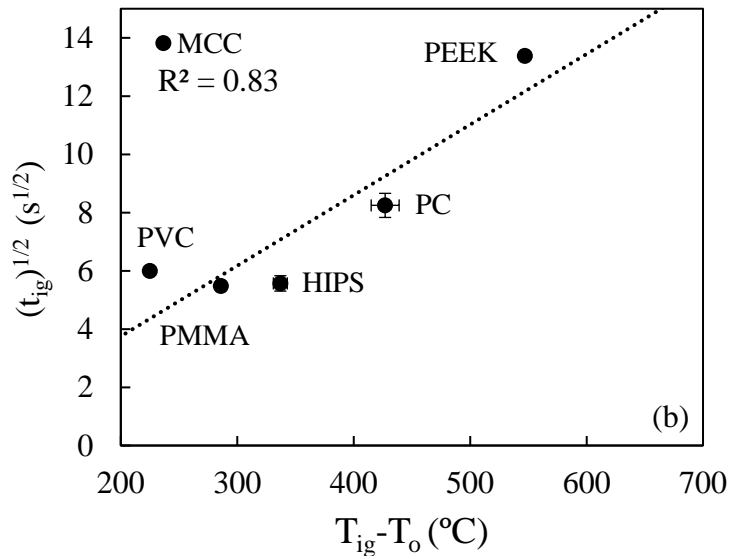
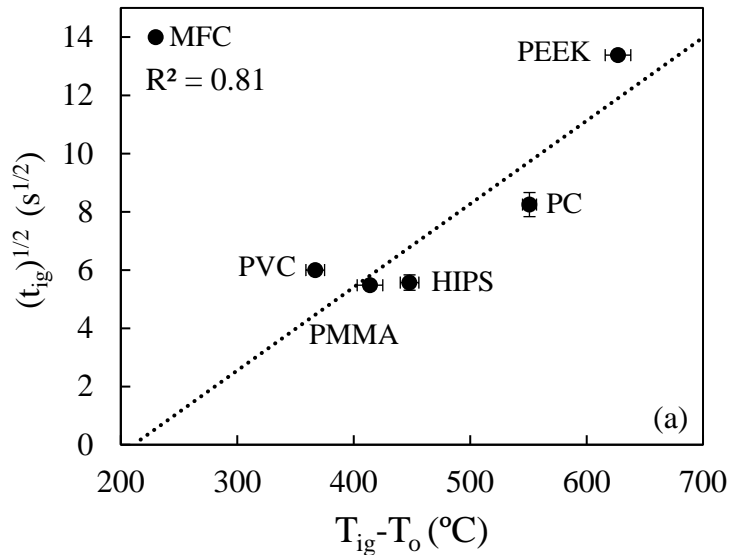


Figure 5.6: Relation between ignition times obtained from cone calorimeter experiments and the ignition temperatures obtained from (a) MFC experiments, (b) the onset HRR temperatures from MCC experiments

It was expected that a high time to ignition value for a material from the cone calorimetry experiments would correspond to a high ignition temperature for that

material. It is noted from Figure 5.6, that on average, the ignition temperature data from the MFC increases as the ignition time data from the cone calorimeter experiments increases. It was further noted that the relationship between the onset HRR temperatures from the MCC ( $R^2 = 0.83$ ) or the ignition temperatures from the MFC ( $R^2 = 0.81$ ) compared to the square-root of the ignition times from cone calorimetry experiments was not perfectly linear. This difference could be potentially be attributed to the assumption of a constant thermal inertia for all the materials as well as the use of different heating rates i.e. incident heat fluxes for different testing techniques.

The ignition temperature values obtained from the MFC experiments was compared to the literature as presented in Table 5.1. This was done to ensure that the measured values were within an acceptable range. The values by Lyon [4] were measured using MCC with the values of Quintiere [30] obtained in the LIFT apparatus

Table 5.1: Comparison of ignition temperatures obtained from the MFC with that presented in the literature

Material	Literature (°C)		MFC ignition temperature (°C)
	Lyon	Quintiere	
PMMA	317	343	439 ± 11
HIPS	413	-	473 ± 8
PEEK	570	580	652 ± 11
PC	500	550	576 ± 6
PVC	395	374	392 ± 8

The onset HRR temperatures obtained from the MCC experiments were directly compared to the ignition temperature from the MFC experiments, as per Figure 5.7. It was noted that the MFC temperatures were always higher than the MCC temperatures. This can be attributed to the heating rates used during MCC and MFC experiments. The heating rate for the MCC is much lower than that in the MFC. The lower heating rate results in a smaller temperature differential between the measured surface temperature of the sample and the temperature of the MCC pyrolyzer. This results in a very small thermal lag between the MCC pyrolyzer and the sample surface. The high heating rate used in the MFC results in a larger temperature differential between the measured temperature of the sample surface and the temperature of the MFC pyrolyzer coil. A larger thermal lag is induced resulting in a higher measured ignition temperature. The thermal insulating effect of char formation during MFC experiments is more accurately captured in the MFC resulting in the shift of the ignition temperatures of the materials shifting to higher values.

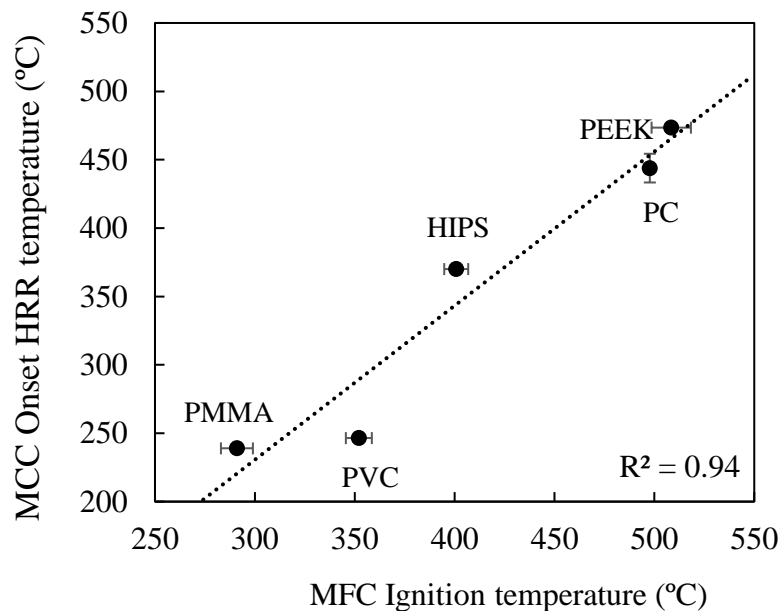


Figure 5.7: Onset HRR temperatures from the MCC experiments compared to the ignition temperatures from the MFC experiments

### 5.5 Smoke yield

The smoke yield for the cone calorimeter experiments was compared to the gravimetric particulate yield for all materials obtained in the MFC. No smoke production was expected in the MCC experiments due to the complete combustion of the sample and was therefore not considered for smoke yield comparative analysis. The particulate yield from the MFC was compared to the average extinction area,  $\sigma_{\text{Average}}$ , from the cone calorimeter with  $\sigma_{\text{Average}}$  indicative of the smoke production during cone calorimetry experiments.

Smoke is defined as a mixture of soot and condensed organic compounds [24] and was measured directly with the use of smoke obscuration measurements in the cone calorimeter. The composition of particulates, for a specific material, that deposits on an MFC particulate filter was assumed to be similar to that of the composition of smoke produced during a cone calorimeter experiment. This assumption allows for the direct comparison of smoke production in the cone calorimeter and the particulate yield using MFC. Least square fitting between the cone calorimeter and MFC data was performed with a linear function as depicted per Figure 5.8.

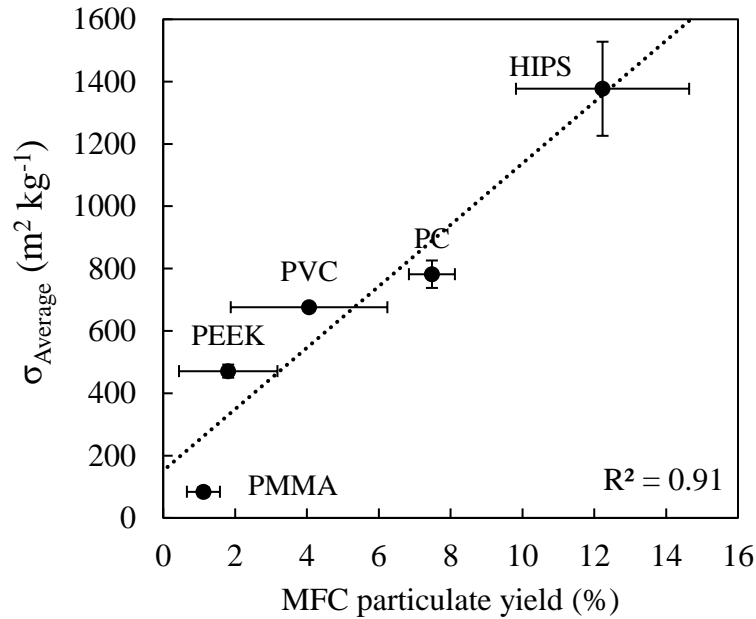


Figure 5.8: MFC particulate yield compared to the average extinction area calculated from cone calorimeter experiments

It was noted that the coefficient of determination was indicative of a strong linear relationship between the average extinction area in the cone calorimeter and the particulate yield in the MFC ( $R^2 = 0.91$ ). This strong relationship suggests that the MFC could be used to predict the smoke production, as normalized by the initial sample mass in the cone calorimeter. The trend also indicates that the burning behavior of materials in the cone calorimeter is captured in the MFC. A large specific extinction coefficient is indicative of a material that produces a large amount of soot particulates during the burning process. HIPS is a sooty material and is expected to have a large specific extinction coefficient or particulate yield. PMMA on the other hand, is expected to

release low concentrations of soot particulates while burning. From Figure 5.8, it is noted that the burning behavior for each of the five materials is adequately captured.



## 6 Conclusions

This study presents the design of a new pyrolyzer system for the MFC which more accurately replicates the one-dimensional heating of a sample in the cone calorimeter. A comparative study of five representative polymeric materials was performed using the MFC with the newly installed pyrolyzer system, the MCC and the cone calorimeter. The pyroprobe pyrolyzer in the MFC was replaced with a more economical pyrolyzer coil that was designed in-house. The new pyrolyzer coil has a flat radial configuration, replacing the spiral coil arrangement of the pyroprobe pyrolyzer. A new ceramic crucible was used to house the sample and was larger than the original crucible. This allowed for the testing of larger samples. The larger sample crucible ensured that the crucible could not be clogged, allowing for the testing of intumescent charring materials. A K-type thermocouple was also added to the pyrolyzer system to enable the direct measurement of sample surface temperature, a feature that was not present in the old MFC instrumentation setup. The setup of the new pyrolyzer system was optimized to ensure prolonged self-sustained flaming combustion of all materials. An updated MATLAB script was used to process the data from the MFC such that the HOC, ignition temperature, time to ignition and peak HRR for a material could be determined.

The performance of the new pyrolyzer coil system was quantified by comparing various flammability parameters obtained from MFC experiments with those obtained using the MCC and cone calorimeter. The char yield and HOC values for each material tested in both the MCC and MFC were directly compared with values obtained from

cone calorimeter experiments. The char yield values obtained in the MFC had a larger uncertainty than that of the MCC values when compared to the cone calorimeter experiments. The HOC values as normalized by the initial sample mass and gasified mass for both the MFC and MCC experiments was compared to the normalized HOC from the cone calorimeter experiments. It was noted that the normalized HOC values for the MFC were very similar to the values obtained using cone calorimetry. This was attributed to MFC more accurately capturing the incomplete flaming combustion behavior of a sample as seen during cone calorimetry experiments. The peak HRR for the MFC experiments using disk-like plates was noted to almost perfectly linearly correlate with the peak HRR values from the cone calorimeter experiments, which is considered to be the most important measure of flammability. However, this was not the case for MCC peak HRR values. The time to ignition data from the cone calorimeter experiments was correlated to the measured surface ignition temperatures for each material in the MFC. The assumption of a thermally thick material was used to compare the results. The linear correlation between the surface ignition temperatures from the MFC and the time of ignition data of the materials obtained during cone calorimeter experiments was reasonable. The particulate yield from the MFC experiments was compared to the average extinction area for each material determined using smoke obscuration measurements in the cone calorimeter. A near linear relationship was observed. This allows for the potential prediction of the average extinction area using particulate yield values from the MFC.

## **7 Future Work**

The future work for this study is to expand the material test matrix to potentially test materials with fillers and flame retardants. The use of a pyrolyzer coil with a temperature range in excess of 750 °C would be beneficial for the testing of composite materials, known to decompose at higher temperatures. A pyrolyzer with a higher temperature range would allow for the use of the same heating rate but the presence of a more prominent temperature inflection point indicative of the self-sustained flaming combustion.

## 8 Bibliography

- [1] S.M.T.A.-T.T.- Halliwell, *Polymers in building and construction*, (2002). <http://site.ebrary.com/id/10236818>.
- [2] J. Swann, *A comprehensive characterization of pyrolysis and combustion of intumescent and charring polymers using two-dimensional modeling: A relationship between thermal transport and the physical structure of the intumescent char*, 2019 TA - TT -, 2019. doi:10.13016/6kol-uubx
- [3] C.D. Papaspyrides, P.T.A.-T.T.- Kiliaris, *Polymer green flame retardants*, (2014). <http://public.ebib.com/choice/publicfullrecord.aspx?p=1770235>.
- [4] R.E. Lyon, M.L. Janssens, U.S.F.A.A.O. of A. Research., S.R. Institute., W.J.H.T.C. (U.S.), *Polymer flammability*, Office of Aviation Research, Federal Aviation Administration ;, Washington, D.C., 2005. <http://purl.access.gpo.gov/GPO/LPS64543>.
- [5] ASTM, *Standard Test Method for Measuring the Comparative Burning Characteristics of Solid Plastics in a Vertical Position*, 2019.
- [6] A.B. Morgan, M. Bundy, *Cone calorimeter analysis of UL-94 V-rated plastics*, *Fire Mater.* TA - TT -. 31 (2007) 257–283. doi:10.1002/fam.937
- [7] M.J. John, Chapter 2 - Flammability performance of biocomposites, in: G. Koronis, A.B.T.-G.C. for A.A. Silva (Eds.), *Woodhead Publ. Ser. Compos. Sci. Eng.*, Woodhead Publishing, 2019: pp. 43–58. doi:<https://doi.org/10.1016/B978-0-08-102177-4.00002-1>.
- [8] ASTM, *Standard Test Method for Measuring the Minimum Oxygen Concentration to Support Candle-Like Combustion of Plastics (Oxygen Index)*, 2017. doi:10.1520/D2863-12.1.
- [9] F. Laoutid, L. Bonnaud, M. Alexandre, J.-M. Lopez-Cuesta, P. Dubois, *New prospects in flame retardant polymer materials: From fundamentals to nanocomposites*, *Mater. Sci. Eng. R Reports.* 63 (2009) 100–125. doi:<https://doi.org/10.1016/j.mser.2008.09.002>.
- [10] R.E. Lyon, R.N. Walters, S.I. Stoliarov, *Screening flame retardants for plastics using microscale combustion calorimetry*, *Polym. Eng. Sci.* 47 (2007) 1501–1510. doi:10.1002/pen.20871.
- [11] ASTM, *Standard Test Method for Determining Flammability Characteristics of Plastics and Other Solid Materials Using Microscale Combustion Calorimetry*,

(2019).

- [12] R.E. Lyon, R.N. Walters, S.I. Stoliarov, Thermal analysis of flammability, *J. Therm. Anal. Calorim.* 89 (2007) 441. doi:10.1007/s10973-006-8257-z.
- [13] M.B. McKinnon, S.I. Stoliarov, Pyrolysis Model Development for a Multilayer Floor Covering, *Materials* (Basel). 8 (2015) 6117–6153. doi:10.3390/ma8095295
- [14] Y. Ding, M.B. McKinnon, S.I. Stoliarov, G. Fontaine, S. Bourbigot, Determination of kinetics and thermodynamics of thermal decomposition for polymers containing reactive flame retardants: Application to poly(lactic acid) blended with melamine and ammonium polyphosphate, *Polym. Degrad. Stab.* 129 (2016) 347–362. doi:https://doi.org/10.1016/j.polymdegradstab.2016.05.014.
- [15] S.I. Stoliarov, F. Raffan-Montoya, R.N. Walters, R.E. Lyon, Measurement of the global kinetics of combustion for gaseous pyrolyzates of polymeric solids containing flame retardants, *Combust. Flame.* 173 (2016) 65–76. doi:https://doi.org/10.1016/j.combustflame.2016.08.006.
- [16] J. Zhuge, X. Chen, A. KS, D.P. Manica, Microscale combustion calorimeter—application and limitation, *Fire Mater. TA - TT -*. 40 (2016) 987–998. doi:10.1002/fam.2358
- [17] F. Raffan-Montoya, X. Ding, S.I. Stoliarov, R.H. Kraemer, Measurement of heat release in laminar diffusion flames fueled by controlled pyrolysis of milligram-sized solid samples: Impact of bromine- and phosphorus-based flame retardants, *Combust. Flame.* 162 (2015) 4660–4670. doi:https://doi.org/10.1016/j.combustflame.2015.09.031.
- [18] C. Hamel, F. Raffan-Montoya, S.I. Stoliarov, A method for measurement of spatially resolved radiation intensity and radiative fraction of laminar flames of gaseous and solid fuels, *Exp. Therm. Fluid Sci.* 104 (2019) 153–163. doi:https://doi.org/10.1016/j.expthermflusci.2019.02.012.
- [19] F. Raffan-Montoya, S.I. Stoliarov, S. Levchik, E. Eden, Screening flame retardants using milligram-scale flame calorimetry, *Polym. Degrad. Stab.* 151 (2018) 12–24. doi:https://doi.org/10.1016/j.polymdegradstab.2018.02.018.
- [20] NIST Reference Fluid Thermodynamic and Transport Properties Database, Version 9.1, (n.d.). <https://www.nist.gov/srd/refprop>.
- [21] C. Dewaghe, C.Y. Lew, M. Claes, S.A. Belgium, P. Dubois, 23 - Fire-retardant applications of polymer–carbon nanotubes composites: improved barrier effect and synergism, in: T. McNally, P.B.T.-P.N.C. Pötschke (Eds.), Woodhead Publ.

Ser. Compos. Sci. Eng., Woodhead Publishing, 2011: pp. 718–745.  
doi:<https://doi.org/10.1533/9780857091390.3.718>.

- [22] C. Huggett, Estimation of rate of heat release by means of oxygen consumption measurements, *Fire Mater.* 4 (1980) 61–65. doi:10.1002/fam.810040202.
- [23] ASTM, Standard Test Method for Heat and Visible Smoke Release Rates for Materials and Products Using an Oxygen, ASTM E 1354-17. (2016).
- [24] P.J. DiNenno, N.F.P. Association., S. of F.P. Engineers., SFPE Handbook of Fire Protection Engineering, 4th ed. /, National Fire Protection Association ;, Quincy, Mass., 2008.
- [25] V. Babrauskas, G.W. Mulholland, Smoke and soot data determinations in the cone calorimeter, (1986).
- [26] G.W. Mulholland, C. Croarkin, Specific extinction coefficient of flame generated smoke, *Fire Mater.* 24 (2000) 227–230. doi:10.1002/1099-1018(200009/10)24:5<227::AID-FAM742>3.0.CO;2-9.
- [27] NFPA, Standard Test Method for Measurement of Flammability of Materials in Cleanrooms Using a Fire Propagation Apparatus, (2017).
- [28] X. Ding, Design and Implementation of the Flaming Combustion Calorimeter, 2013 TA - TT -, 2013. <http://hdl.handle.net/1903/14906>.
- [29] W.J. Meredith, J.B. Massey, Fundamental physics of radiology, LK - <https://umaryland.on.worldcat.org/oclc/2616563>, Wright, Bristol SE - viii, 599 pages 411 illustrations, plan 26 cm, 1968.
- [30] J.G. Quintiere, Principles of fire behavior LK - <https://umaryland.on.worldcat.org/oclc/36509994>, Delmar Publishers, Albany, N.Y. SE - xi, 258 pages: illustrations; 24 cm, 1998. <http://catdir.loc.gov/catdir/enhancements/fy1215/97011199-t.html>.
- [31] J.G.T.A.-T.T.- Quintiere, Fundamentals of fire phenomena, (2006). doi:10.1002/0470091150